

Raman mapping: Introduction and application to the imaging of zircon textures

Dr. Tamás VÁCZI
Department of Mineralogy
Eötvös Loránd University, Budapest

C.V. Raman's spectrographs



C.V. Raman



Sir Chandrasekhara Venkata Raman
inelastic scattering of visible light,
experimental proof: 1928

Nobel Prize: 1930

“... the new field of spectroscopy has practically unrestricted scope in the study of problems related to the structure of matter.”

(Nobel lecture, 1930)

MAY 5, 1928]

NATURE

711

or with the simple gun harpoon usually die at the surface and float, while those killed with the bomb harpoon, as is well known, usually do so under water and sink. The latter appear to do so because death is seldom instantaneous enough to prevent them leaving the surface, yet the injury done them is usually so serious that they are unable to regain it and consequently die under water from asphyxia.

ROBERT W. GRAY.

33 The Strand, Exmouth.

The Optical Analogue of the Compton Effect.

THE presence in the light scattered by fluids, of wave-lengths different from those present in the incident light, is shown very clearly by the accompanying photographs (Fig. 1). In the illustration (1)

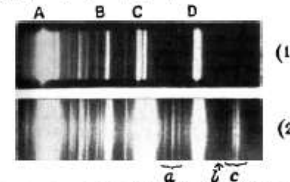


FIG. 1.—(1) Spectrum of incident light; (2) spectrum of scattered light.

represents the spectrum of the light from a quartz mercury vapour lamp, from which all wave-lengths greater than that of the indigo line have been filtered out. This line (4358 Å.) is marked D in the spectrogram, and C is the group of lines 4047, 4078, and 4109 Å. Spectrogram (2) shows the spectrum of the scattered light, the fluid used being toluene in this case. It will be seen that besides the lines present in the incident spectrum, there are several other lines present in the scattered spectrum. These are marked a, b, c in the figure, and in addition there is seen visually another group of lines which is of still greater wave-length and lies in a region outside that photographed. When a suitable filter was put in the incident light to cut off the 4358 line, this latter group also disappeared, showing that it derived its origin from the 4358 line in the incident radiation. Similarly, the group marked c in spectrogram (2) disappeared when the group of lines 4047, 4078 and 4109 was filtered out from the incident radiation by quinine solution, while the group due to 4358 Å. continued to be seen. Thus the analogy with the Compton effect becomes clear, except that we are dealing with shifts of wave-length far larger than those met with in the X-ray region.

As a tentative explanation of the new spectral lines thus produced by light-scattering, it may be assumed that an incident quantum of radiation may be scattered by the molecules of a fluid either as a whole or in part, in the former case giving the original wave-length, and in the latter case an increased wave-length. This explanation is supported by the fact that the diminution in frequency is of the same order of magnitude as the frequency of the molecular infra-red absorption line. Further, it is found that the shift of wave-length is not quite the same for different molecules, and this supports the explanation suggested.

Careful measurements of wave-length now being made should settle this point definitely at an early date.

C. V. RAMAN.
K. S. KRISHNAN.

210 Bowbazar Street,
Calcutta, Mar. 22.
No. 3053, VOL. 121]

Excitation of the Auroral Green Line in Active Nitrogen.

THE auroral green line, which is now thought to be an arc line of oxygen, has been excited with considerable intensity in active nitrogen that was produced by a condensed discharge in a mixture of nitrogen and about 4 per cent. oxygen. Under the most favourable conditions for its excitation, the line was as intense as the afterglow band at 5442 Å. Eastman astronomical plates were used because of their great sensitivity in the green. The spectrum was photographed on a small Hilger visible spectrograph. Because of the small dispersion of the instrument, the wave-length of the line could be measured only to within 0.1 Å. Using helium standards the wave-length was found to be 5577.5 Å. The measurements of Babcock and of others give this wave-length as 5577.35 Å. It was shown definitely that with decreasing amounts of oxygen the line gradually disappeared. This and the fact that the wave-lengths agree fairly well, give sufficient proof that the line in question is the auroral green line.

Besides the green line, a red line having a wave-length of 6854.8 Å. was observed in the afterglow under the same conditions as the green line. There is an unclassified line of oxygen at 6654.8 Å. and it is thought that these two lines are identical. Amounts of oxygen too small to bring out the green line were found to be sufficient to bring out the red line. This observation is based on the fact that the red line was as intense as one of the afterglow bands in the red (6185 Å.), the intensity of which was given by Lord Rayleigh as the same as the band 5442 Å. mentioned in connexion with the green line.

Too little is known about the energy levels of the oxygen atom and about the spectroscopic origin of the green line for any hypothesis as to the process of excitation in this experiment to be of any value. The excitation of the line with an intensity comparable with that of one of the afterglow bands does, however, seem to indicate that the dissociation of the oxygen molecule and the excitation of the atom occur in a single act. Since no green line afterglow has ever been observed in oxygen discharge tubes, it is certain that the excitation in this experiment is due to the active nitrogen. It is interesting that the green line has been excited without the simultaneous excitation of the other strong arc lines of oxygen, a phenomenon that occurs in the night sky, where the green line alone has been observed.

JOSEPH KAPLAN,
(National Research Fellow in Physics.)
Palmer Physical Laboratory,
Princeton University, U.S.A.
April 13.

Stellar Radiation and the Nature of the Universe.

REFERRING very briefly to NATURE of April 28, p. 674, the reason Dr. Jeans and I agree to differ in our estimate of the possibilities of the universe is because he is dependent on matter for all energy, the rest being empty space; whereas I postulate a vast store of energy in a rotational ether, which only or mainly manifests itself in localised portions apprehended by us as particles or waves.

Similarly, a cyclically permanent universe would seem to him dull or dead; whereas to me it furnishes the mechanism apparently needed for the continued evolution of an entity known to us as life or mind, which, unlike its inorganic counterpart, is progressive.

OLIVER LODGE.

Today's laboratory spectrometers



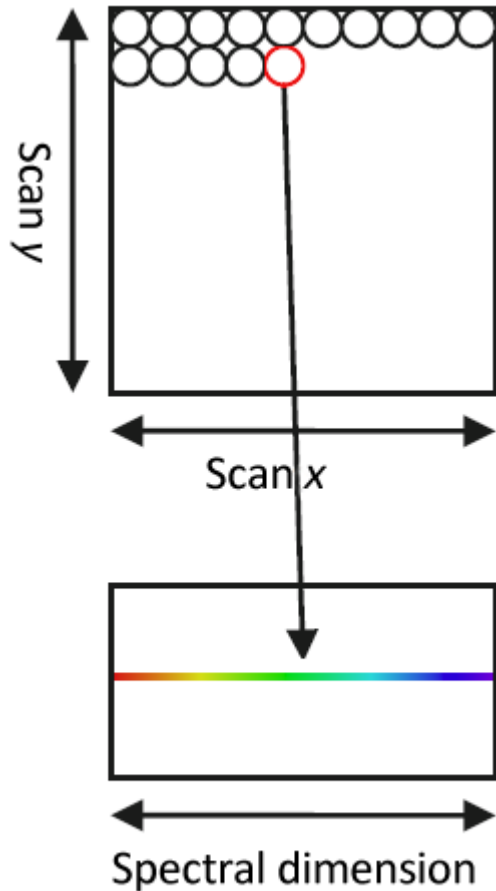
Not shown:

- computer driving motorised/piezo-driven stage that enables collecting and processing multidimensional data sets
- user (!!!)

HOW?



Mapping

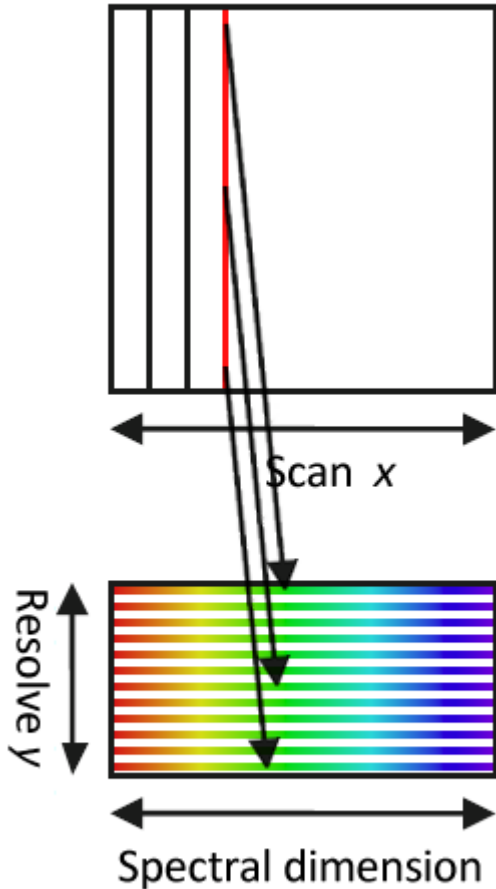


Mapping using **point focus**:

“oD” illumination, spot stepped in a raster

- “true confocal” microscopy
- best optical performance at the cost of throughput
- excellent to good spectral selectivity
- good depth selectivity

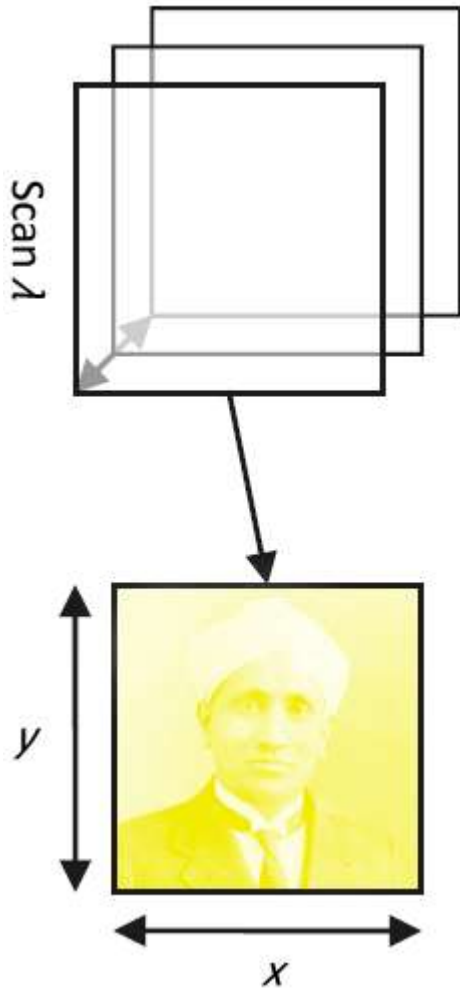
Fast mapping



One of several fast mapping options: **line focus**
“instantaneous” in 1D; line profile stepped across surface

- “pseudo-confocal” microscopy
- used for high-speed mapping (or less beam damage)
- excellent to good spectral selectivity
- good depth selectivity

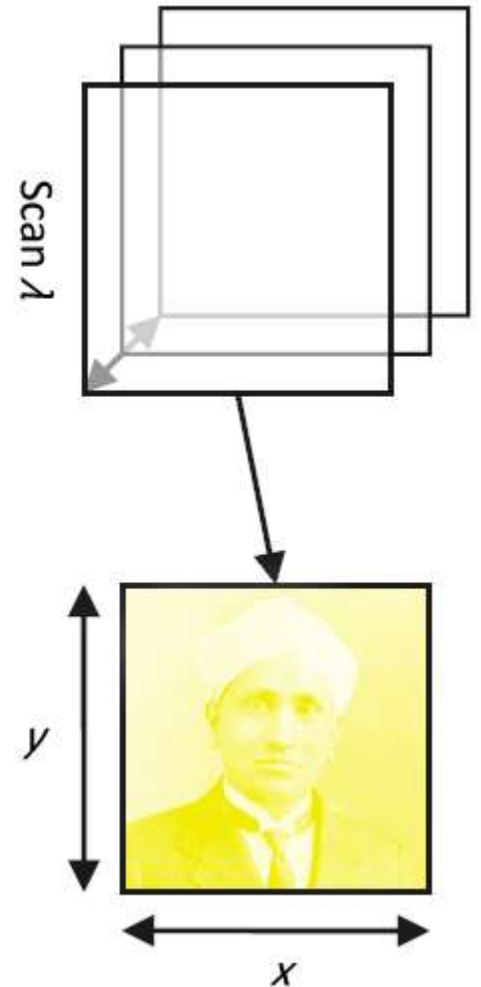
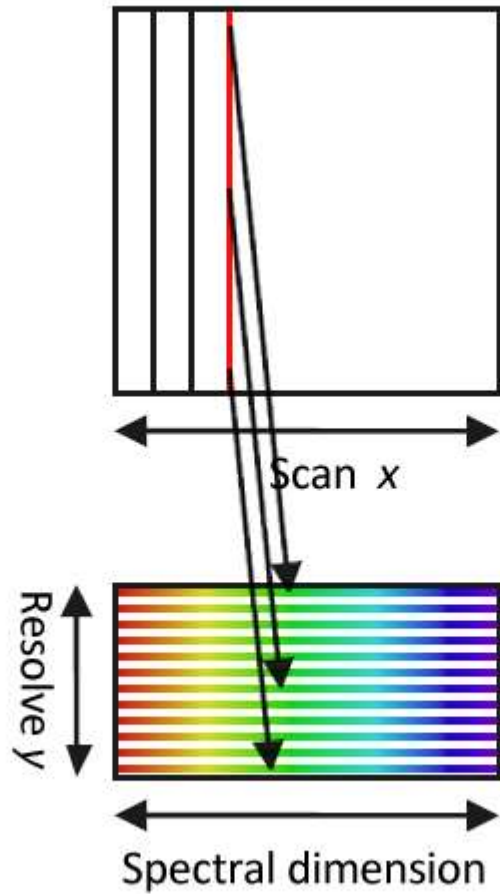
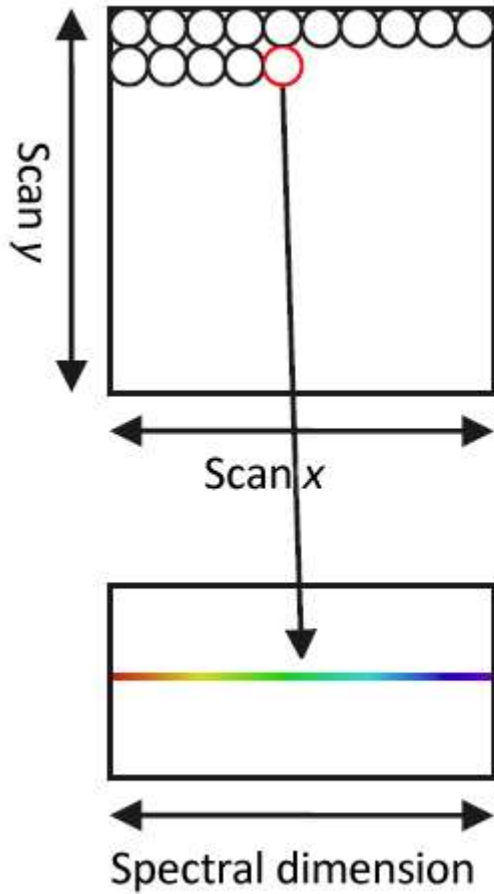
Imaging



Multispectral or hyperspectral direct imaging:
“instantaneous” 2D images.

- homogeneous, global illumination
- needs special band pass filter device (e.g. LCTF)
- good for high-throughput screening, remote sensing etc.
- moderate to poor spectral selectivity
- no depth selectivity, no below-surface imaging


Mapping vs. imaging



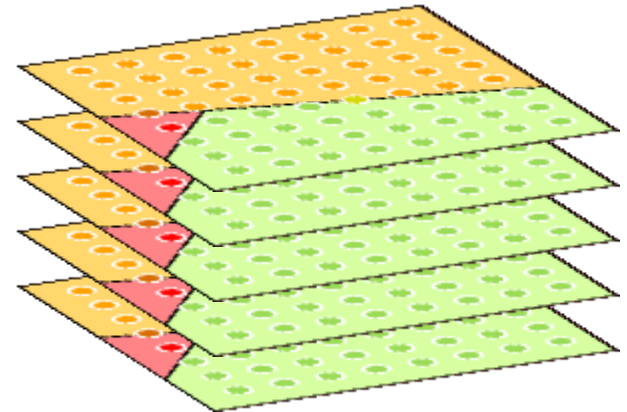
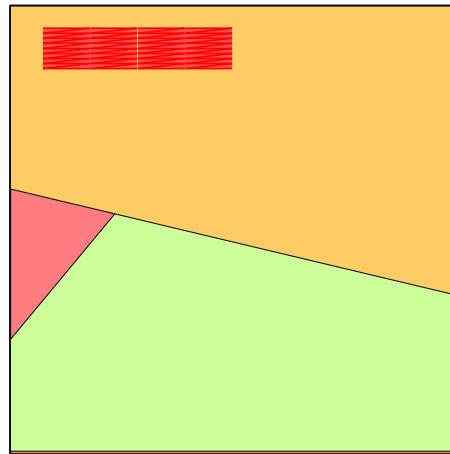
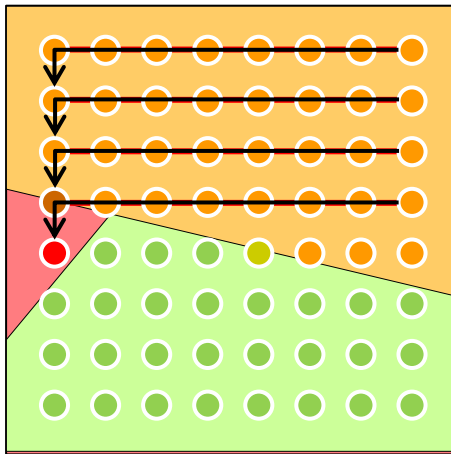
modified from Lee (2012)

Sampling methods

We map a surface through rastering the sampling spot (map).

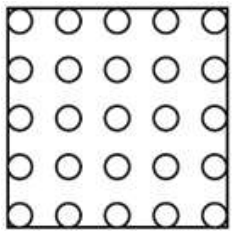
- Stage (sample) moves under a stationary beam
- Laser beam stepped over sample – limited by FOV, vignetting
- Combined techniques  can cover gaps between steps or decrease damage

3D: raster — focus — raster — focus — raster ...



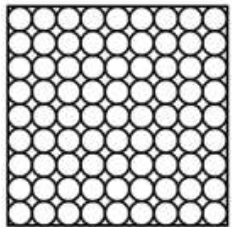
Choosing step sizes

Nyquist criterion: signal variation should be sampled at half the intervals of the *smallest expected feature size* (originally frequency)



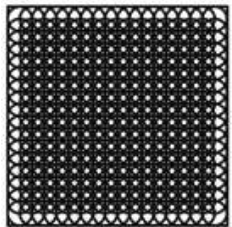
undersampling

fast & good to cover large area at the risk of missing small features



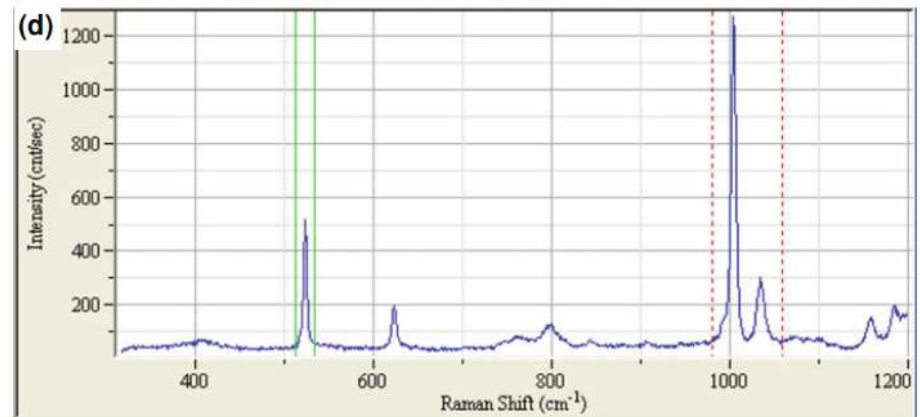
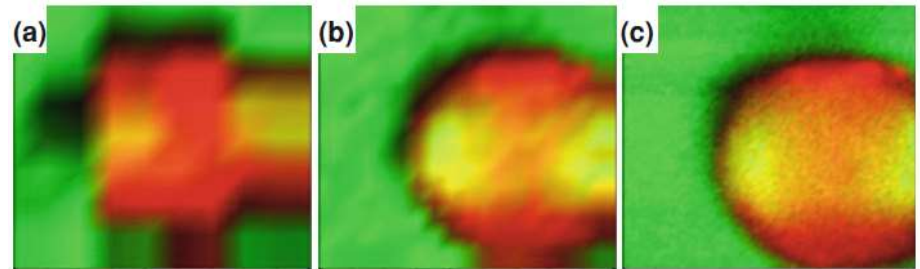
par-sampling

best match to spot size



oversampling

best definition of shapes



from Lee (2012)

$\lambda = 532 \text{ nm}$; (a) $1 \mu\text{m}$; (b) $0.5 \mu\text{m}$; (c) $0.1 \mu\text{m}$

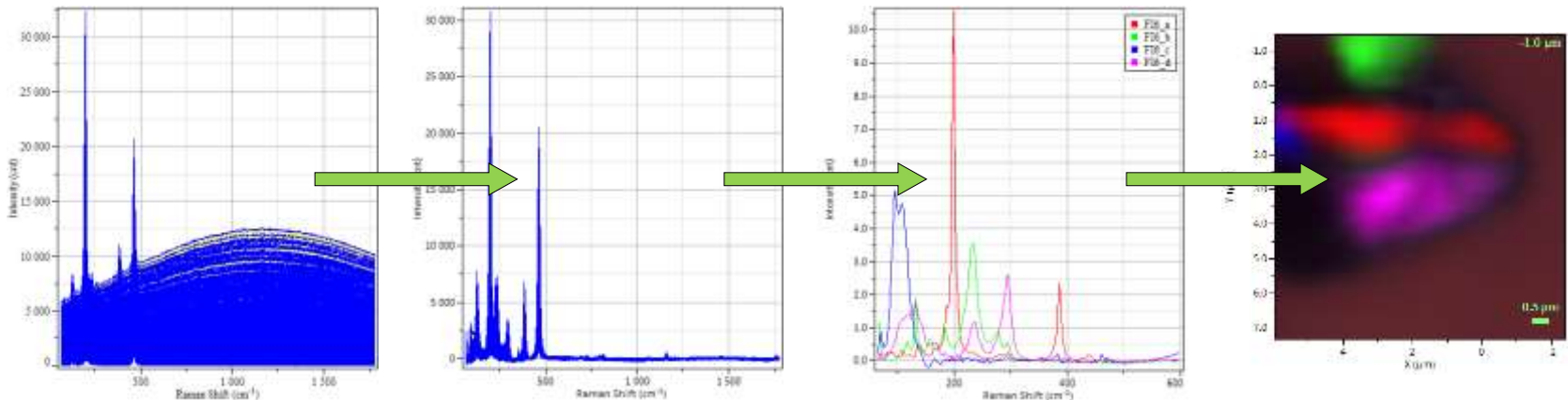
Similar concerns exist for z (depth). There is an ugly time penalty for small step sizes!

Data reduction

Purpose: convert data to information (spatial info from a large number of spectra).

To create informative imagery from raw data several steps may be necessary:

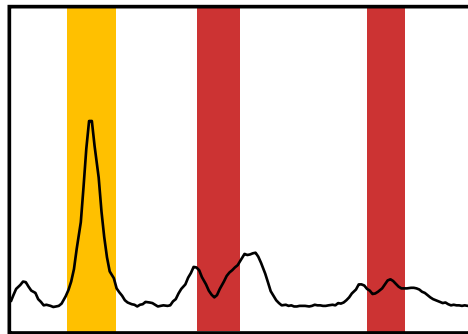
- [CRE/spike elimination, smoothing]
- background subtraction – you may want to use the background (PL) signal!
- image generation
- corrections, adjustments
- analysis
- publication
- happiness!



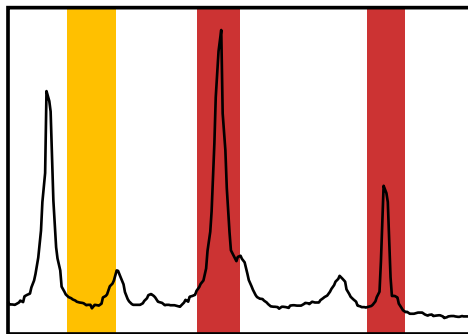
Data reduction: creating images

Raman maps are multidimensional data sets: each x,y pixel/ x,y,z voxel contains a Raman spectrum. Raw maps are only viewable with dedicated spectroscopy software, to visualize chemical/physical content we need to process them.

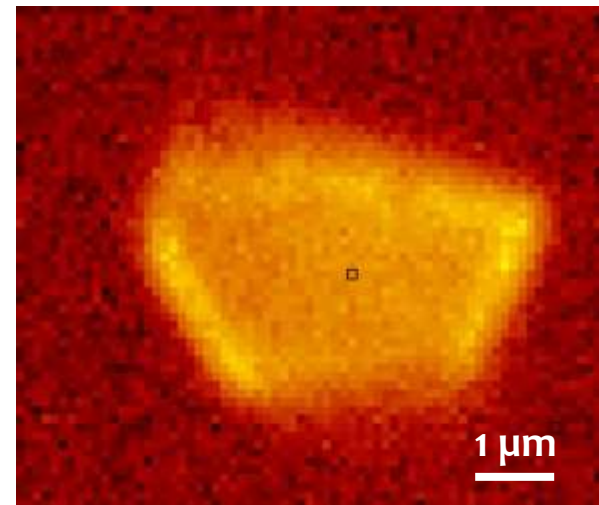
1. **Integral intensities:** uses the integral of the signal between two limits (cursors), with or without “baseline” subtraction, to display a *basic distribution of a few components* – only good for intensities



phase A



phase B

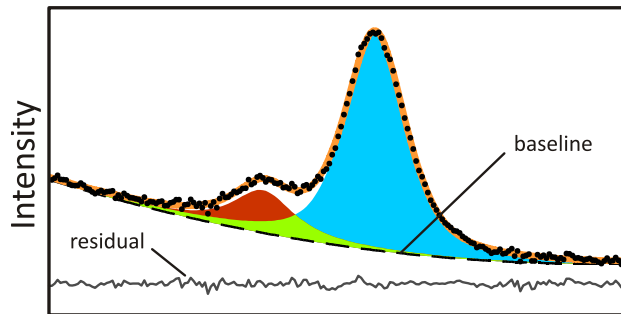


NH₄-Fe/Al sulfates

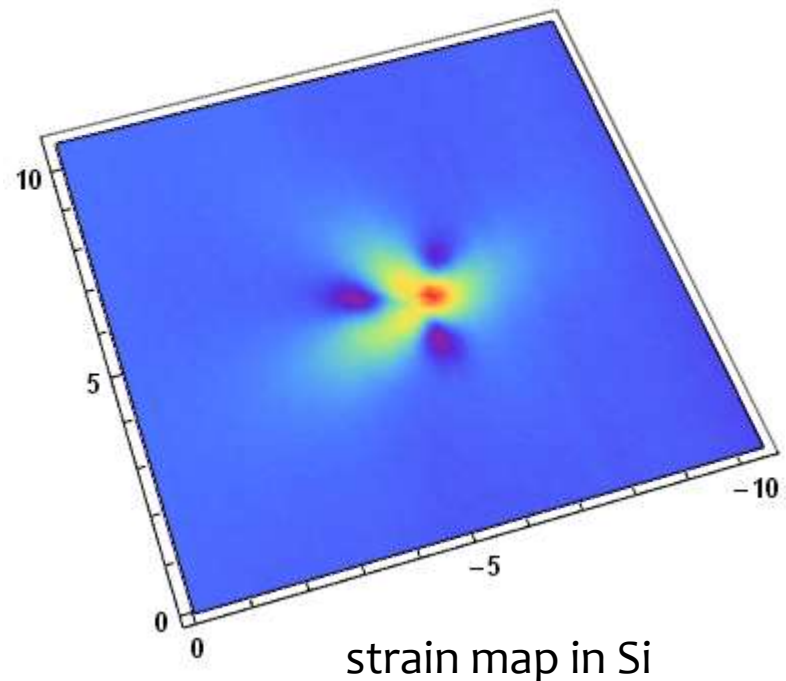
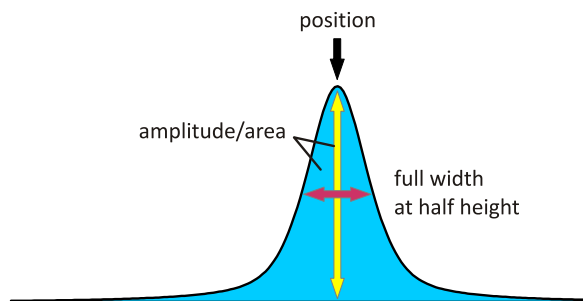
Data reduction: creating images

Raman maps are multidimensional data sets: each x,y pixel/ x,y,z voxel contains a Raman spectrum. Raw maps are only viewable with dedicated spectroscopy software, to visualize chemical/physical content we need to process them.

- Spectral parameters** (position, intensity, FWHM): uses parameters from individual, fitted analytical profiles to display *phase distribution, quantitative physical and chemical properties and their changes*



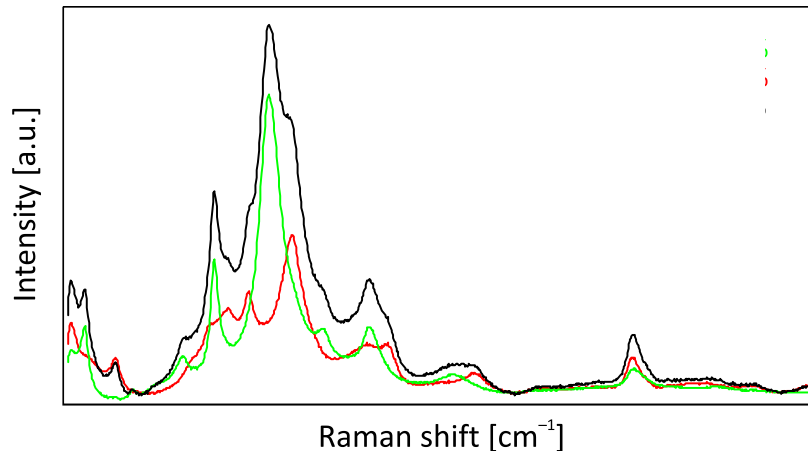
Raman shift



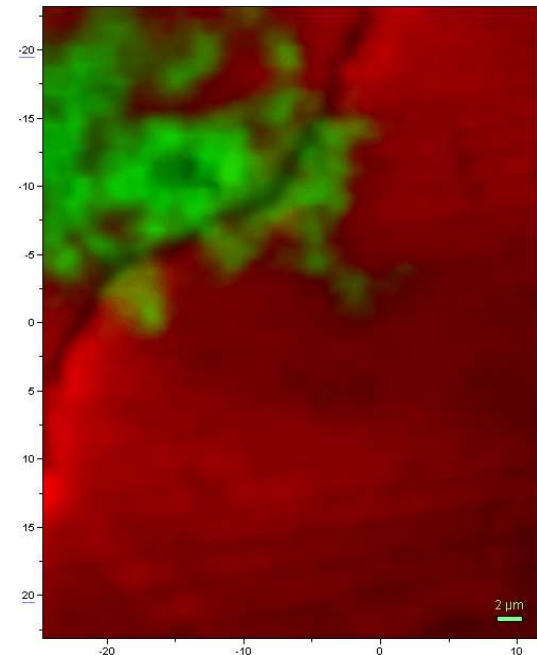
Data reduction: creating images

Raman maps are multidimensional data sets: each x,y pixel/ x,y,z voxel contains a Raman spectrum. Raw maps are only viewable with dedicated spectroscopy software, to visualize chemical/physical content we need to process them.

- Multivariate analysis:** uses entire spectra to decompose multiple/mixed spectra, to display *subtle variations* or a *distribution of many phases* — *good treatment of mixed spectra and broad bands*



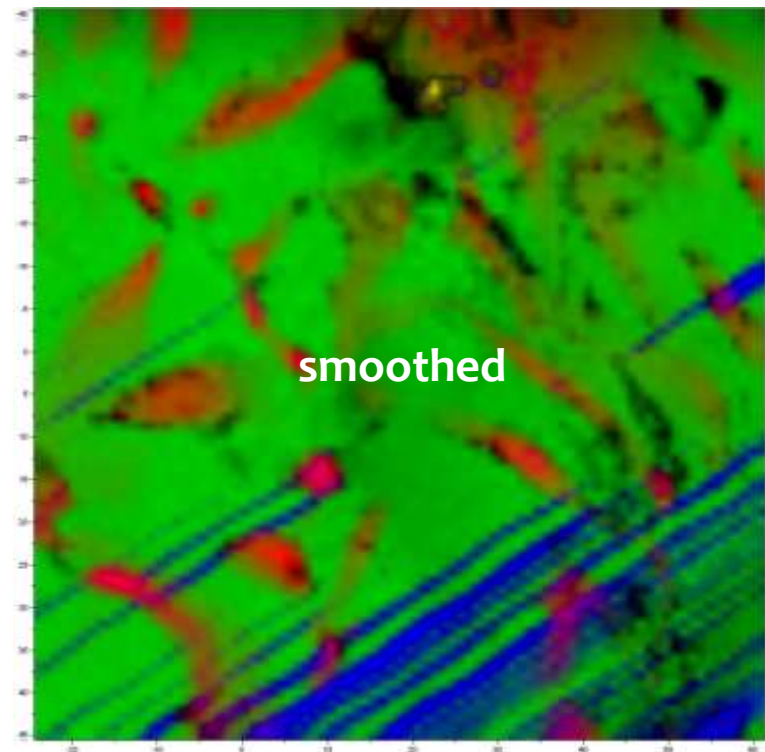
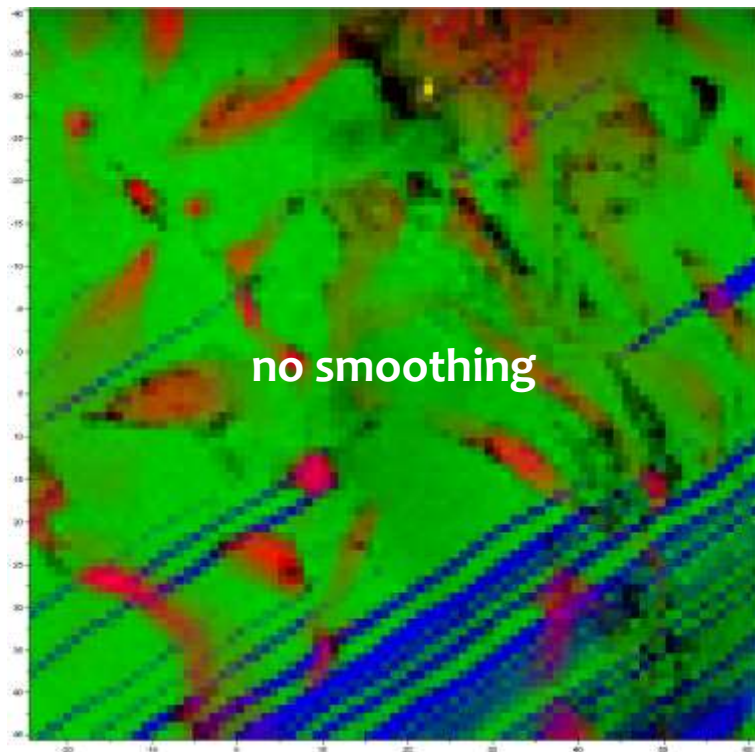
supervised DCLS fitting of
a linear combination of model spectra



schwertmannite, goethite

Image smoothing (blurring)

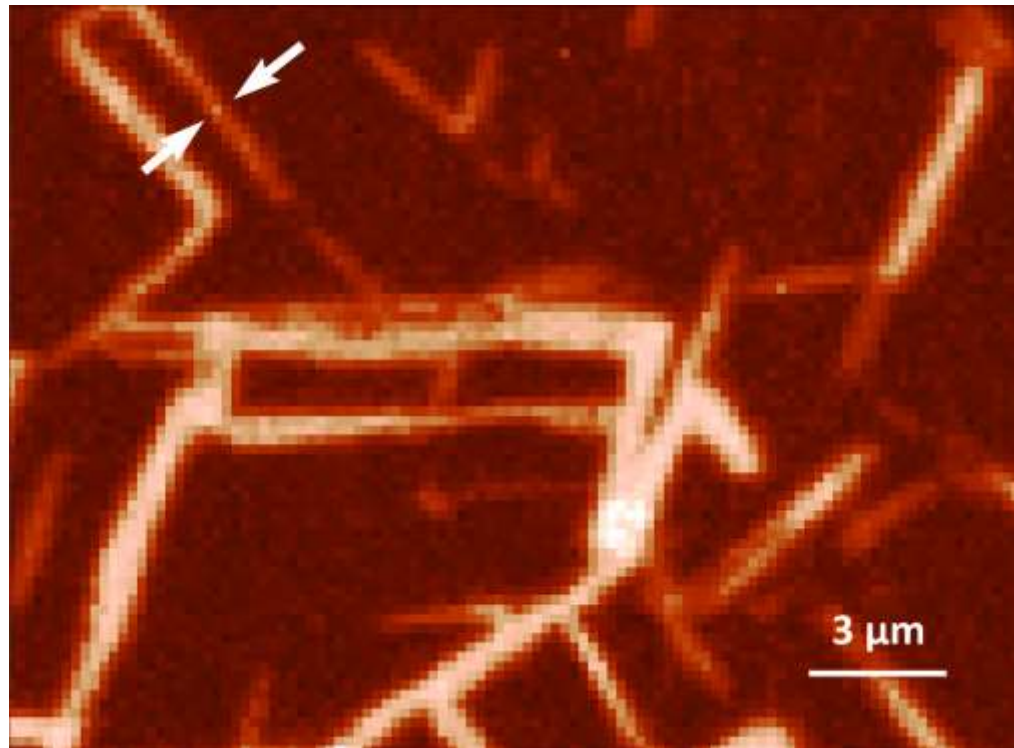
May show a more appealing view of the same image by blurring pixel edges (similar to antialiasing) — **no change in data!**



Myrmekite from the Duluth Complex (Minnesota). A DCLS fit can distinguish between **quartz**, **feldspar** and different **feldspar orientations**.
(532 nm, ~40 mW, 2×2.5 s, 85×85 steps/1 μm)

Resolution

The best achievable resolution is determined by the spot size and the desired contrast.



Black inclusion in serpentinite: hematite in magnetite.

The thickness of the marked lamella is $0,29 \mu\text{m}$
(473 nm , N.A. 0.9 , $d_R = 0.32 \mu\text{m}$, 4 s , $109 \times 80 \text{ steps}/0.2 \mu\text{m}$).

WHAT?



What?

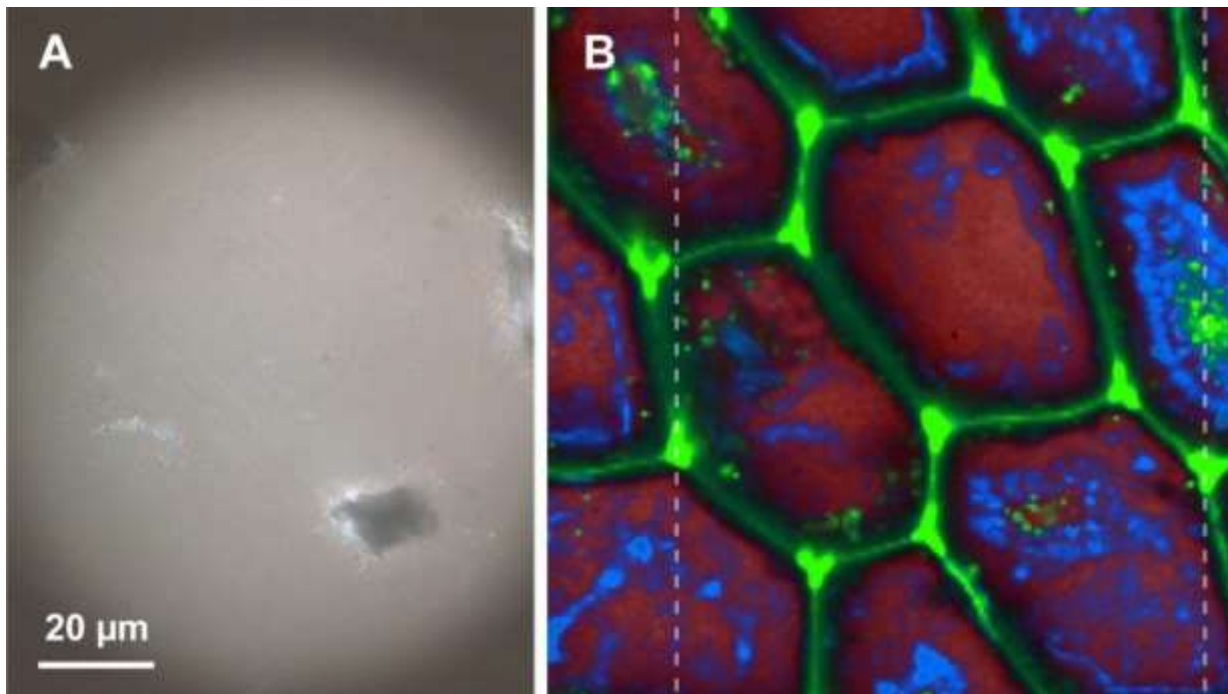
We create images in which contrast comes from identity. You can display a *distribution of anything that can be derived from single spectra*: intrinsic chemical and/or physical properties.

- structure
- composition
- strain
- order, defects
- crystal orientation
- grain size
- grain shape
- ...
- ...
- ...

Through mapping you may get location bias out of the picture and move towards representative and quantitative distribution information.

Phase distribution

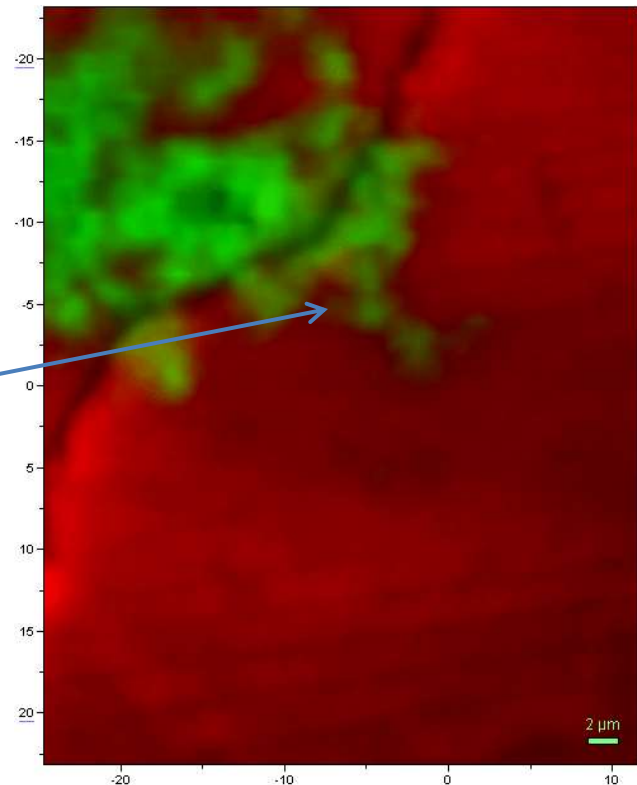
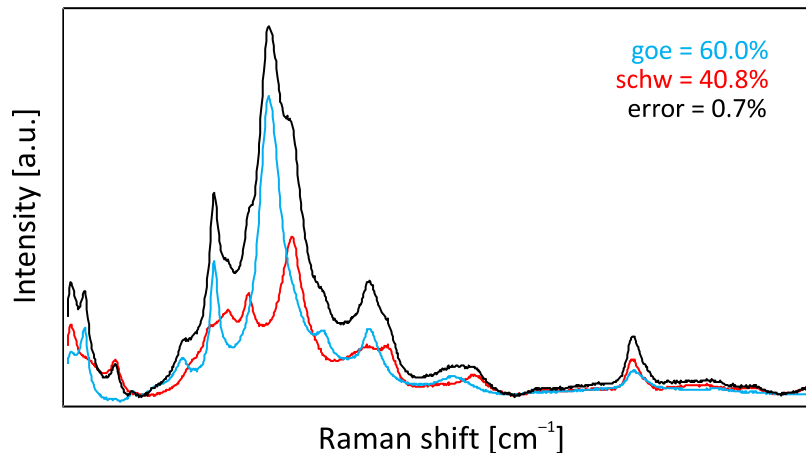
Tree opal from Megyaszó (NE Hungary): no detail in reflected-light microscope, but very well distinguishable on a chemical image (mixed Raman/PL map, 473 nm).



red: opal
green: strong PL emission
blue: C-H_x vibrations (artefact?)

Phase distribution

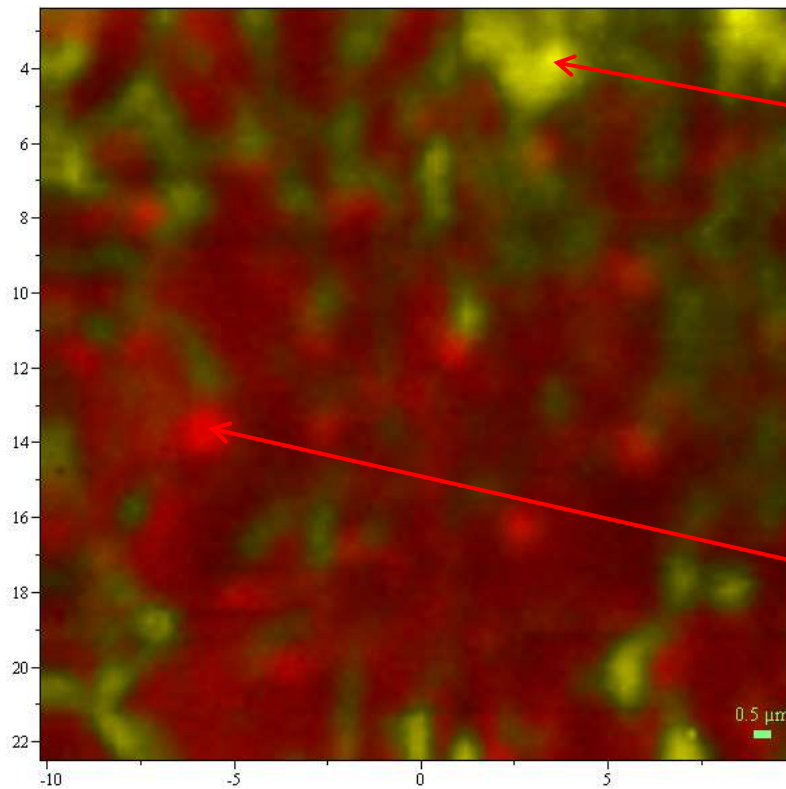
Iron-rich crust on a rock fragment from the Bányabérc waste dump, Mátra Mts., Hungary. As a result of subaerial weathering processes in an acidic environment, crusts of iron oxide-hydroxides, oxy-hydroxide-sulfates and sulfates formed. (633 nm, ~1.3 mW, 2×10 s, 90×115 steps/0.4 μm)



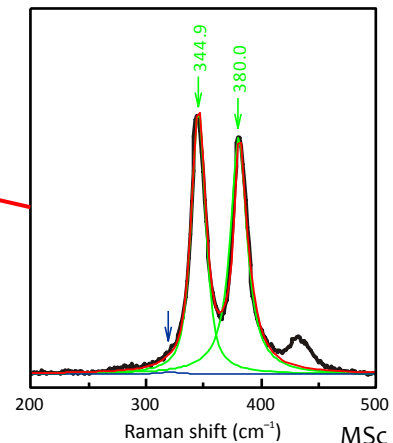
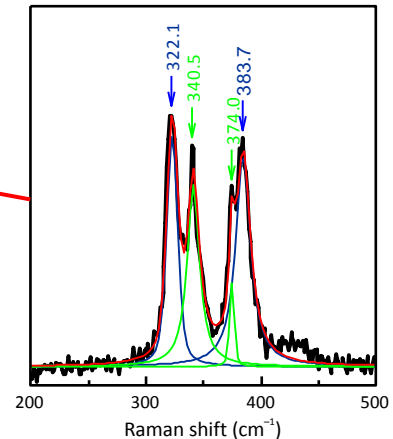
phase map (goethite, schwertmannite)

Phase distribution

Submicrometre association of pyrite and marcasite (colloform pyrite) from Parádfürdő (Recsk Ore Complex, NE Hungary). Due to minor band shifts (heating?), DCLS fitting was inappropriate. Note that optical resolution is insufficient for this material. (633 nm, ~3.3 mW, 2×10 s, 100×100 steps/0.2 μm)

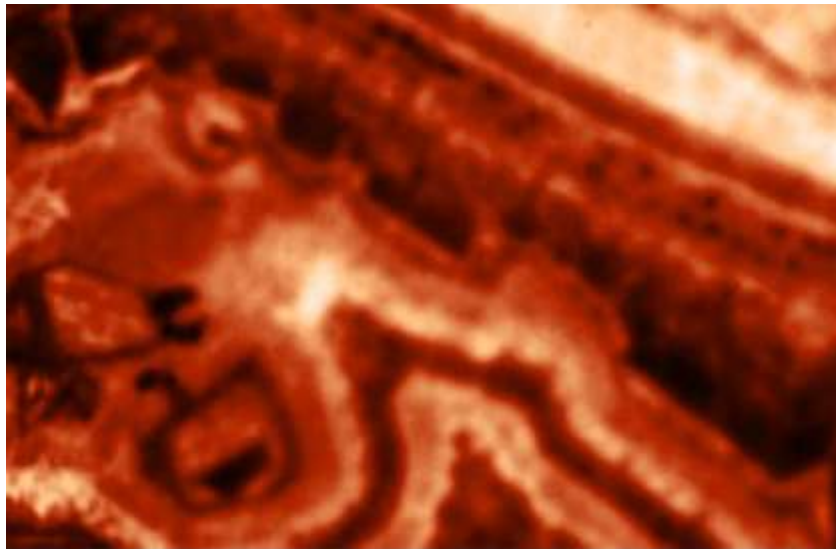


phase map (pyrite, marcasite)

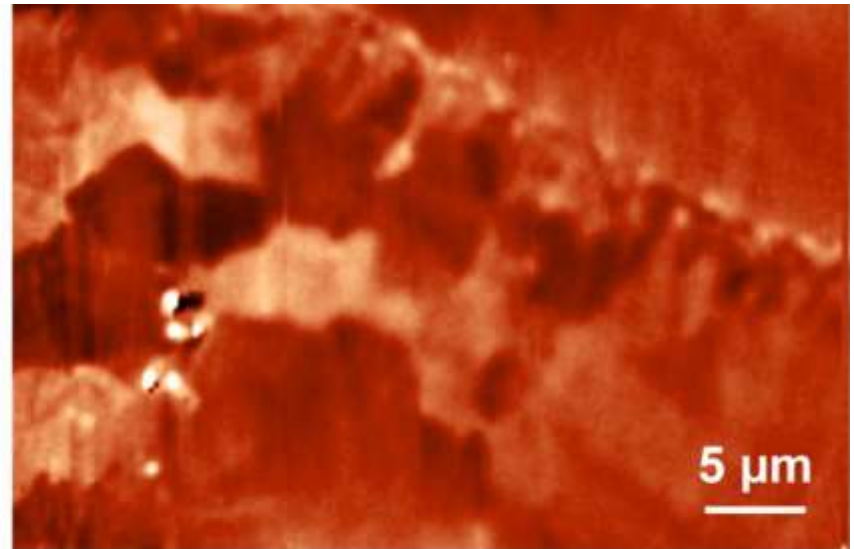


Chemical zoning, crystal orientation

Pyrite with anomalously high Pb content (Bor area, Serbia, sample courtesy A. Pacevski). The two Raman maps show the same area!



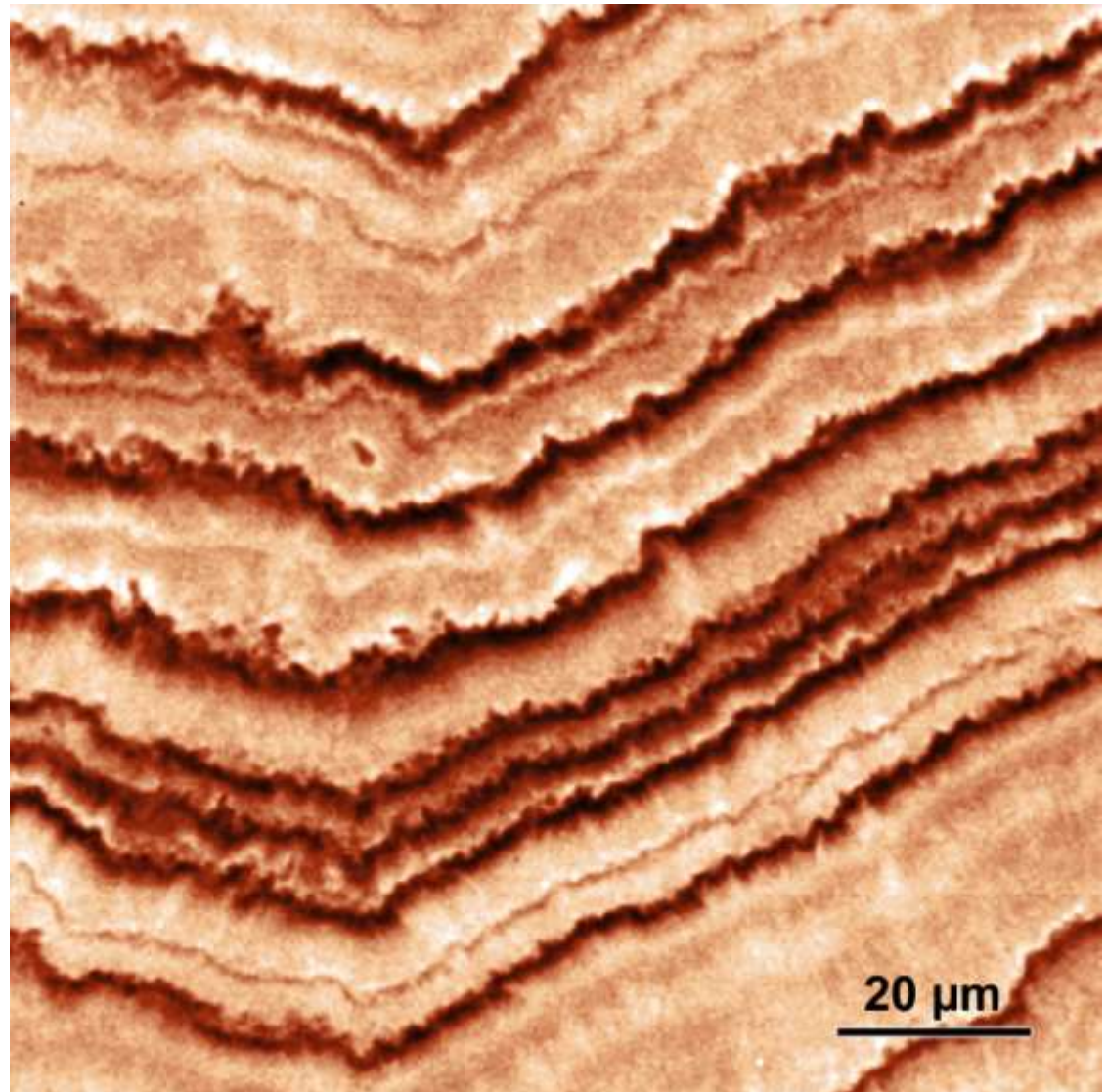
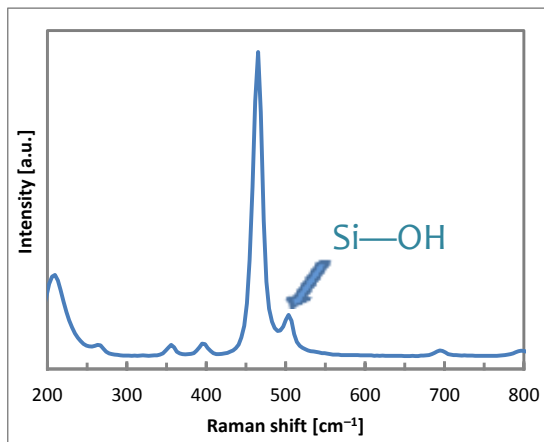
map constructed from
band position



map constructed from
band area

Crystal defects

Chalcedony growth zones:
map constructed from the
intensity of the Si—OH
defect band (@503 cm⁻¹)
(Schmidt et al., 2012)

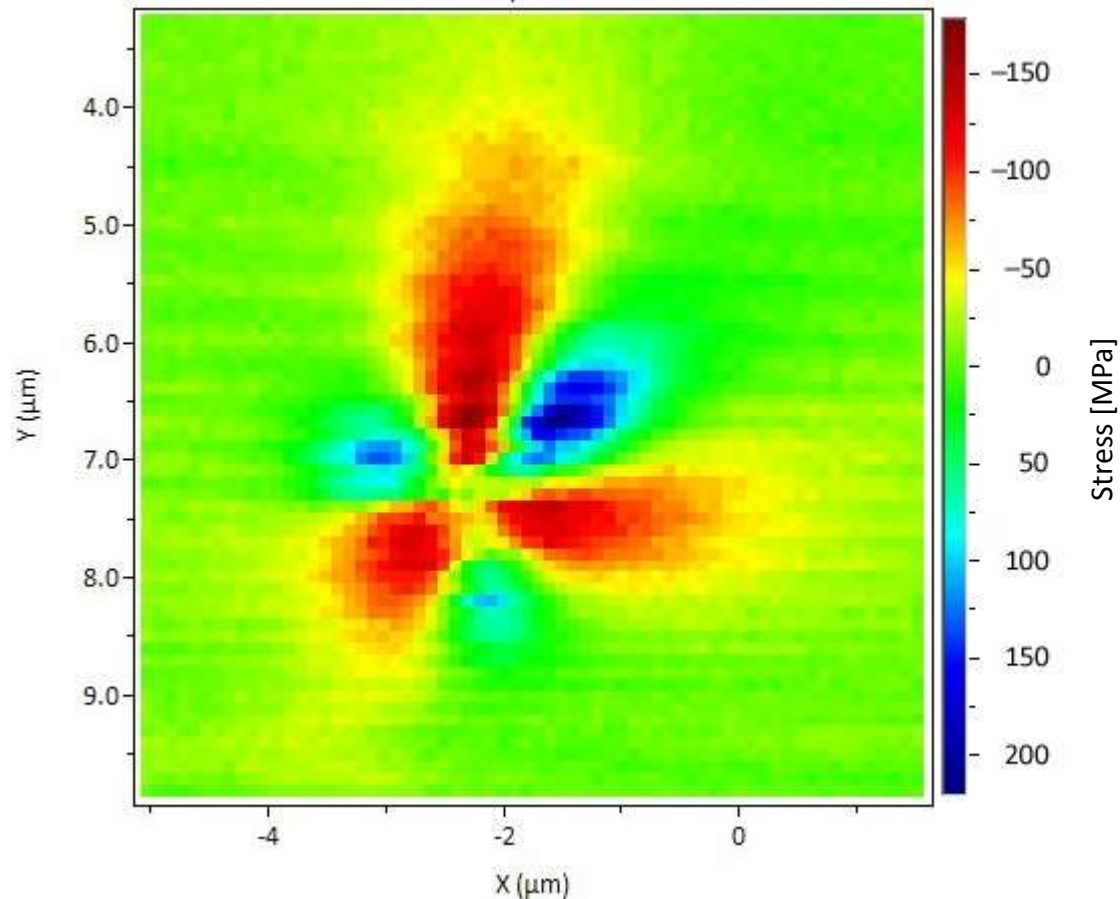


Strain map

Nanoindenter impression in single-crystal silicon (Berkovich tip, 20 mN).

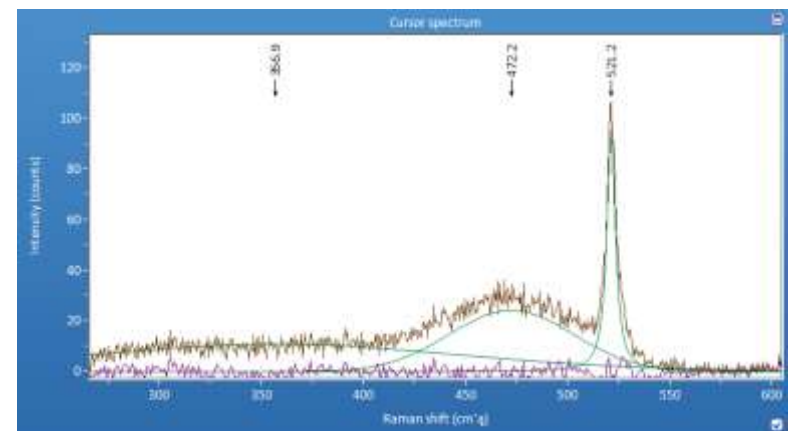
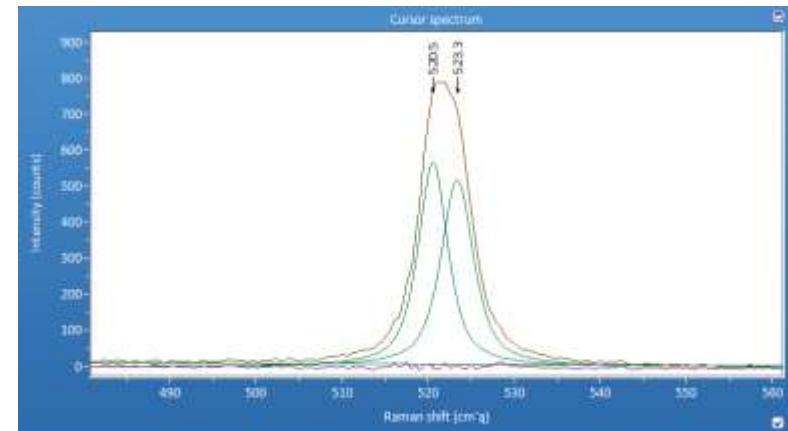
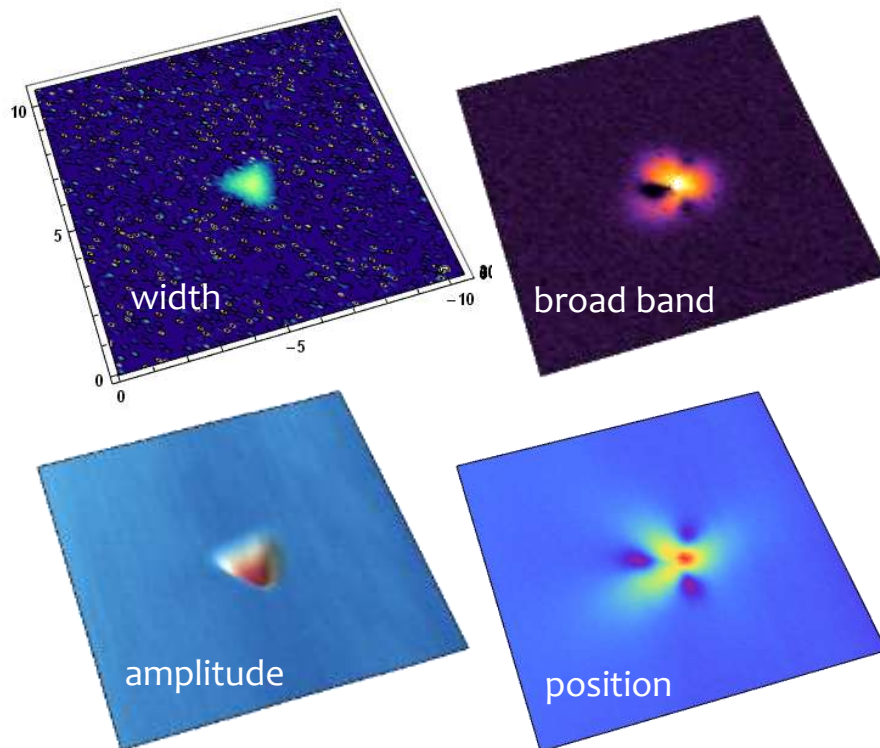
Assuming uniaxial stress, band shift is convertible into strain: $+1 \text{ cm}^{-1} = -500 \text{ MPa}$.

I. De Wolf (1996) *Semicond. Sci. Technol.* **11**:139



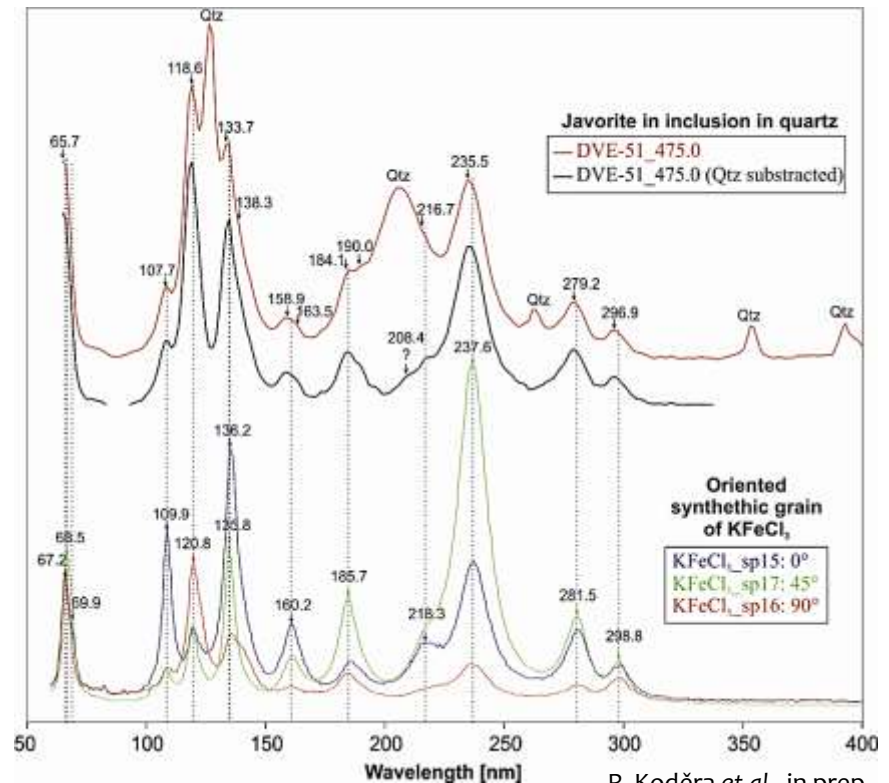
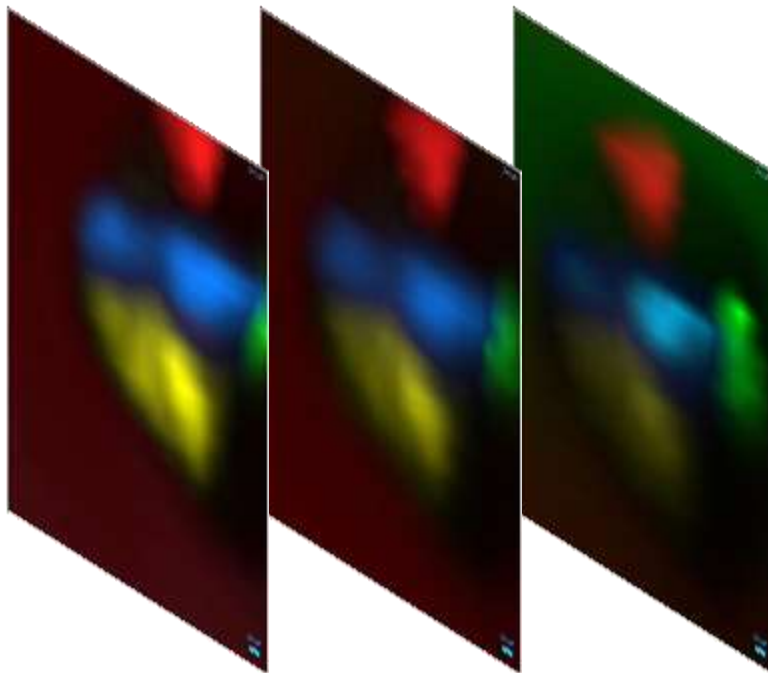
Strain map

Nanoindenter impression in single-crystal silicon (Berkovich tip, 20 mN). In addition to strain haloes, further analysis reveals deviatoric stress and amorphous Si. (633 nm, ~4 mW, 2×1.5 s, 108×106 steps/0.1 μm)



3D mapping: new mineral!

Salt melt inclusion in an unusual, Cu-free Au-porphyry deposit (Biely Vrch, Javorie Stratovolcano, Slovakia). 3D mapping was helpful to locate the purest spectra of salts (still, spectrum subtraction was necessary). Raman analysis confirmed the analogy of the *new mineral javorieite* (IMA 2016-020) with synthetic KFeCl_3 . (532 nm, ~40 mW, 4×3 s, 32×29 x-y steps/0.3 μm , 3 z steps/1.0 μm)

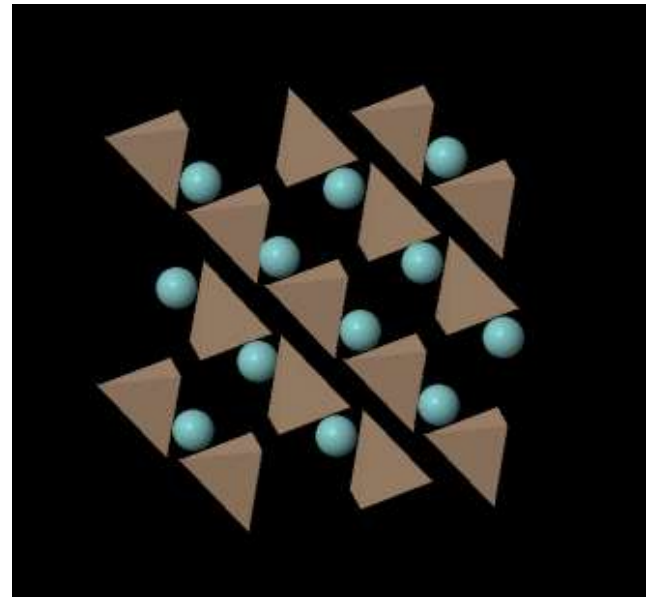
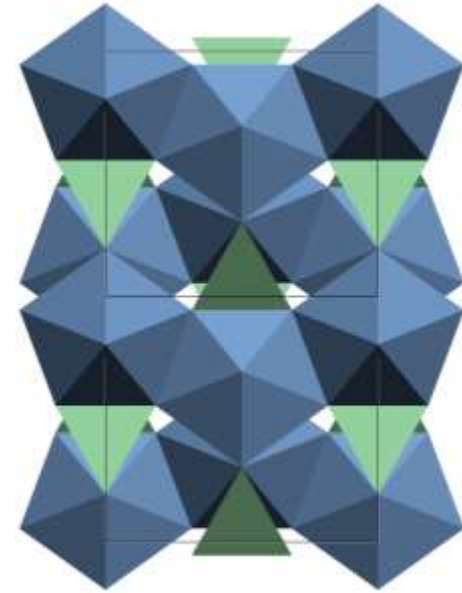


Raman imaging of zircon

Zircon

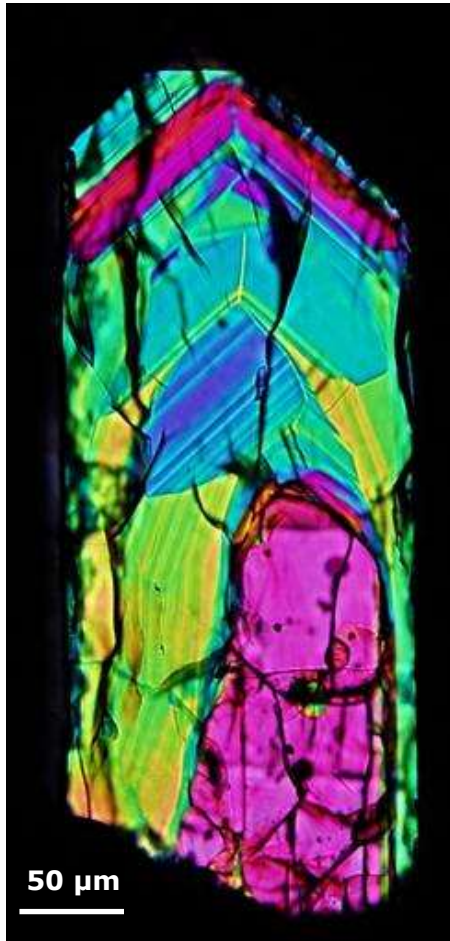
zircon

- ZrSiO_4 ($Z = 4$)
- $I4_1/amd$
- ortho/nesosilicate
- Zr site: ZrO_8
compatible with
large HFS elements
(Hf, REE, U, Th)
- Si site: SiO_4
P, 4H
- interstitial sites



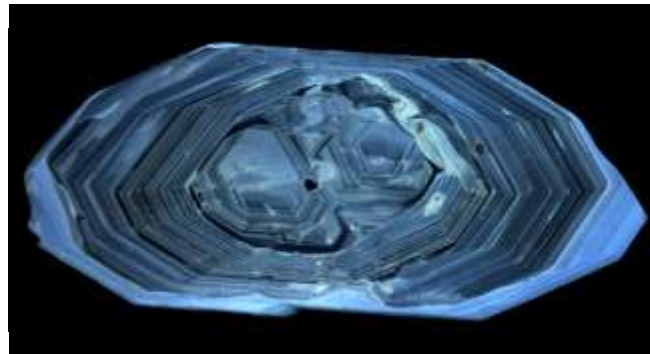
Zircon textures

PLM



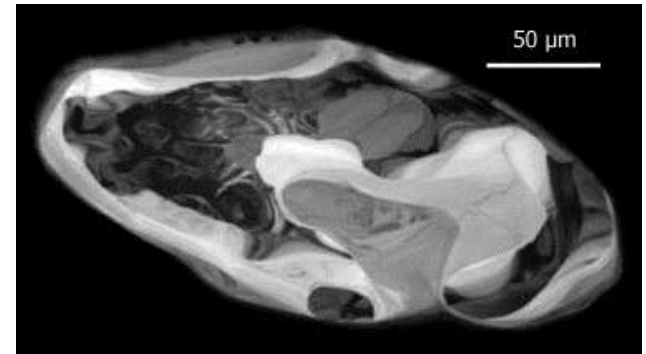
Nasdala et al. (2005)

CL

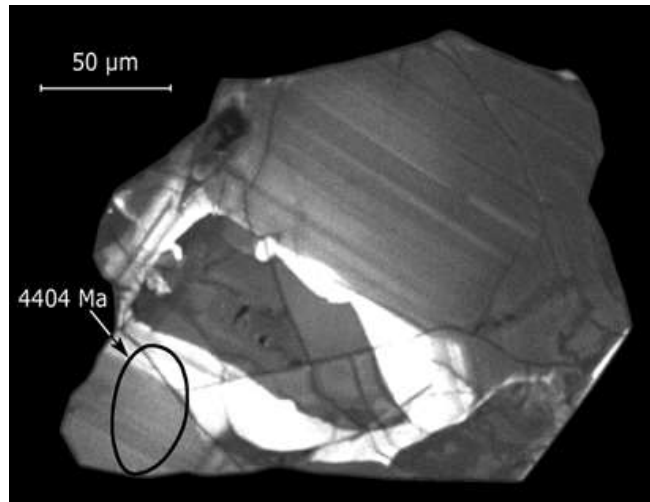


Arizona LaserChron Center

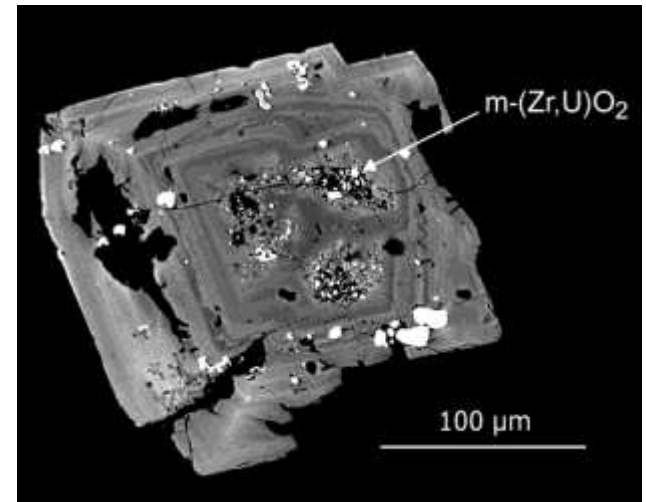
BSE



Ireland & Williams (2003)



J.W. Valley (Peck et al., 2000)



Geisler et al. (2005)

Raman spectroscopy: structural state

Increasing radiation damage:

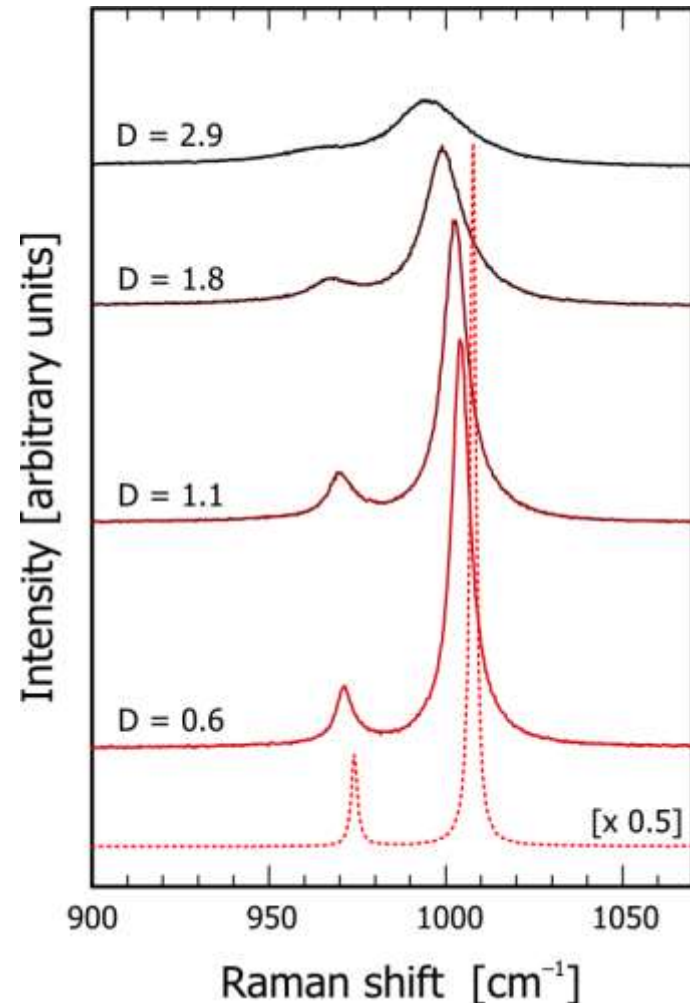
- intensity loss
- peak shift
- **band broadening**
- amorphous fraction
- (new peaks)

Dose (D): 10^{18} alpha events/g

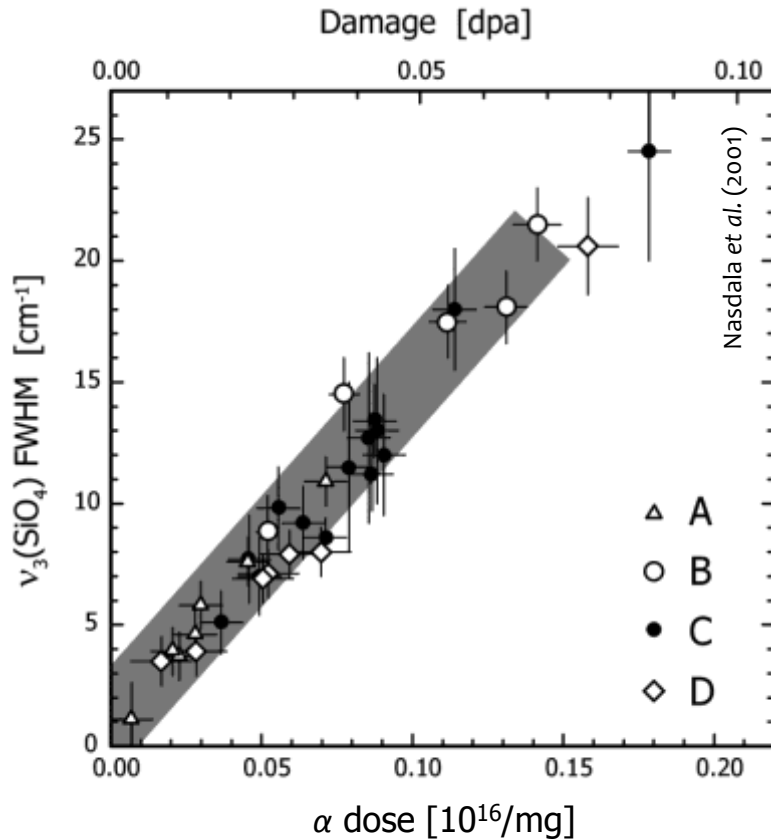
- U & Th concentrations
- age

Naturally accumulated damage

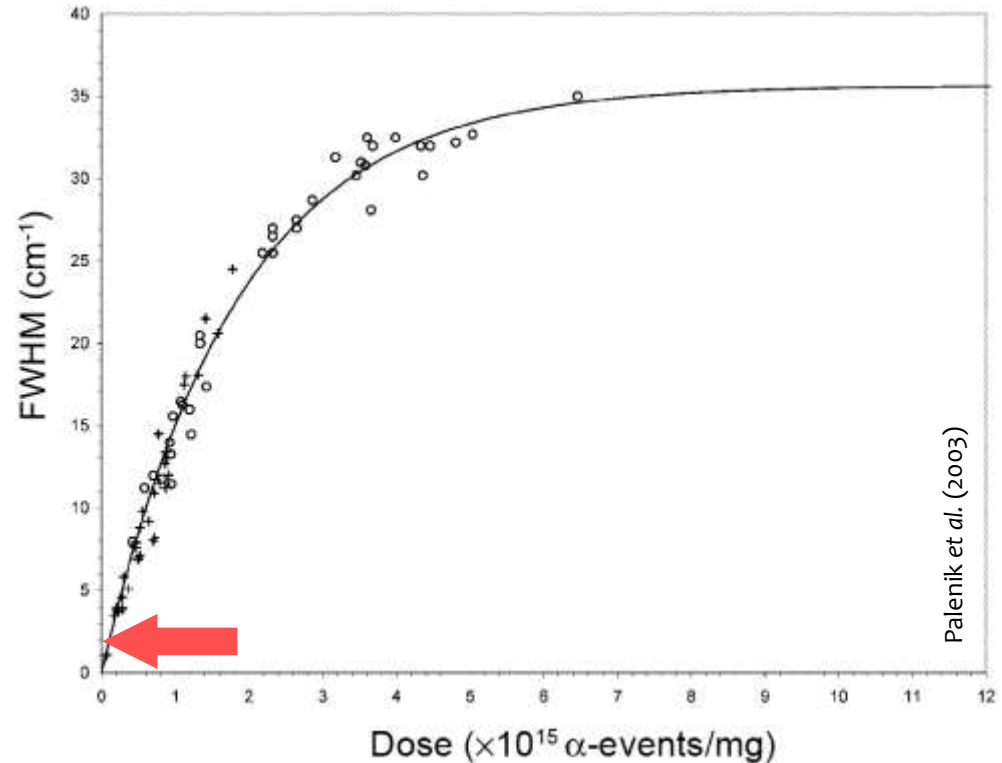
- dose
- thermal history (!)



Raman spectroscopy: structural state

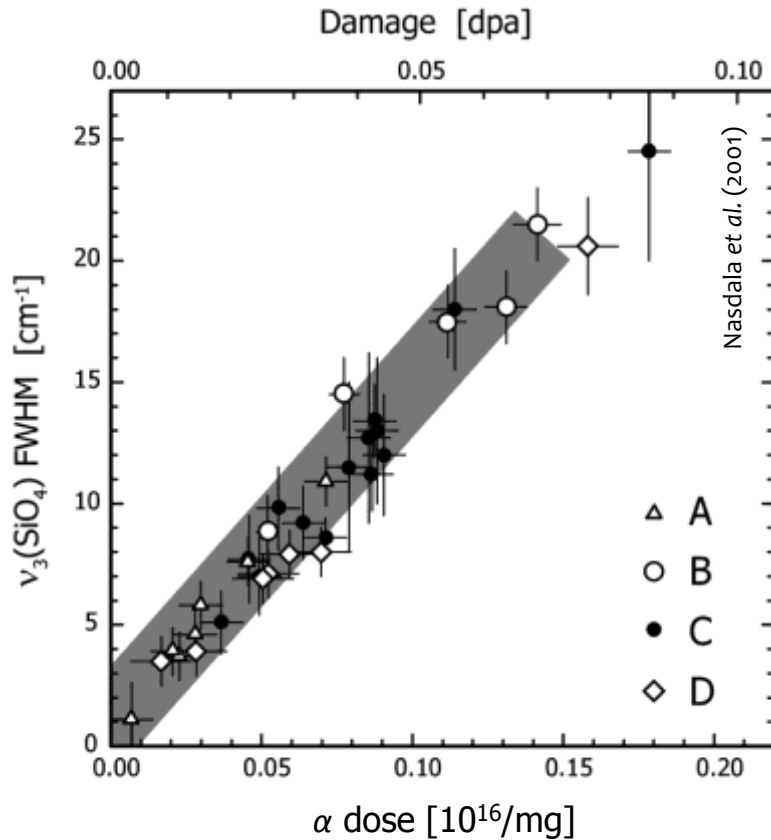


A: Saxonian rhyolite
B: Moon
C: Meissen massif monzonite
D: Frankenstein gabbro

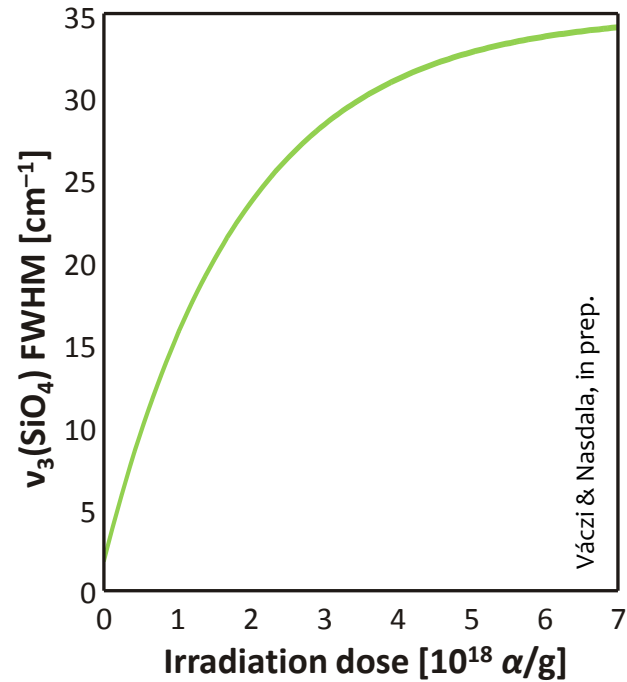


+ : un-annealed zircon
○ : Sri Lankan zircon (*effective dose*,
corrected for thermal annealing)

Raman spectroscopy: structural state



A: Saxonian rhyolite
 B: Moon
 C: Meissen massif monzonite
 D: Frankenstein gabbro



+ : un-annealed zircon
 ○ : Sri Lankan zircon (effective dose, corrected for thermal annealing)

BSE contrast in zircon

Nasdala et al. (2006) *Am. Mineral.* **91**:1739

BSE contrast

Sources of contrast in back-scattered electron (BSE) images

- BSE signal intensity is *qualitative* and *relative*:
brightness, contrast are adjusted until *image looks just fine*

backscattering coefficient η :
fraction of primary electrons
emitted from sample surface

- BSE yield is a strong function of the average atomic number (\bar{Z}):
“composition contrast”

$$\bar{Z} = \left(\sum_i c_i \sqrt{Z_i} \right)^2$$

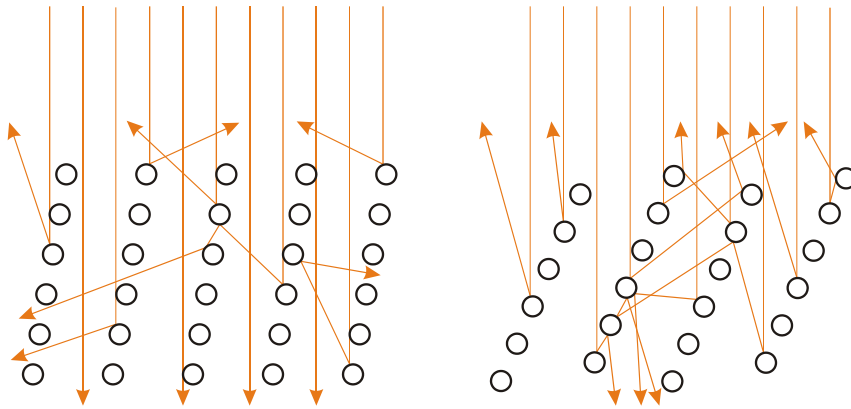
$$\bar{\eta} = 1.75 \cdot 10^{-3} \bar{Z} + 0.37 \left[1 - \exp(-0.015 \cdot \bar{Z}^{1.3}) \right]$$

according to Pouchou & Pichoir (1991)

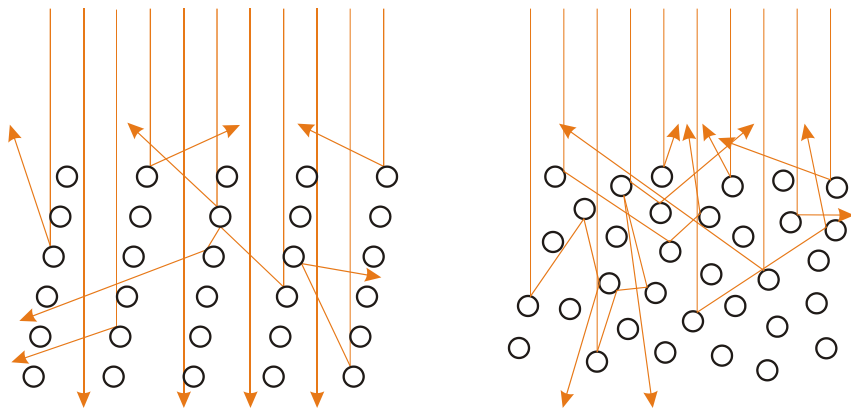
BSE contrast

Sources of contrast in back-scattered electron (BSE) images

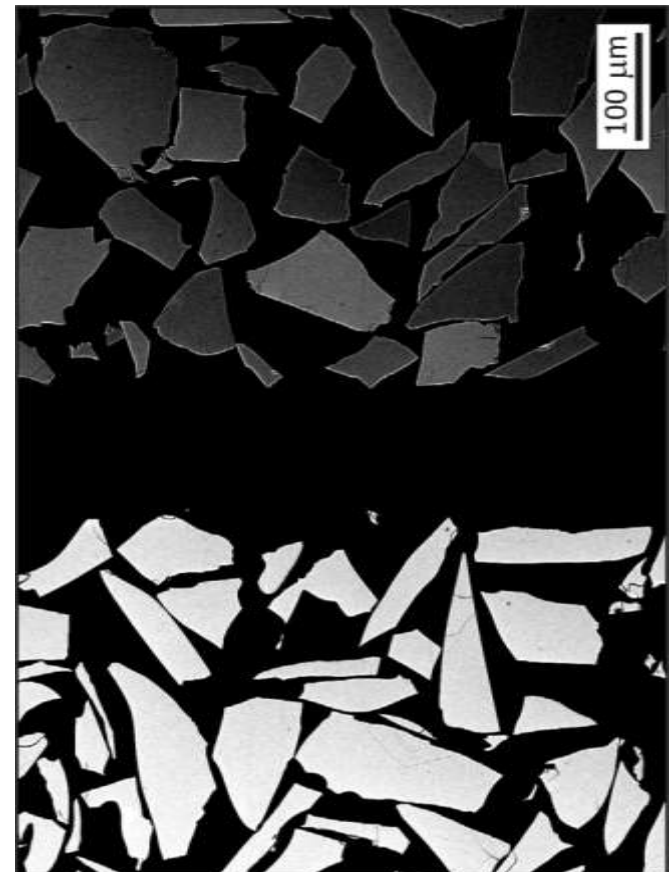
- crystallographic contrast



orientation contrast



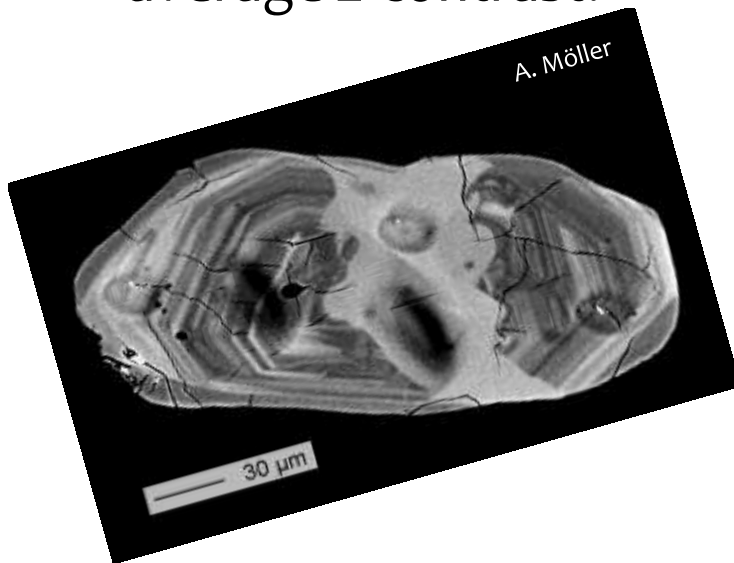
phase contrast



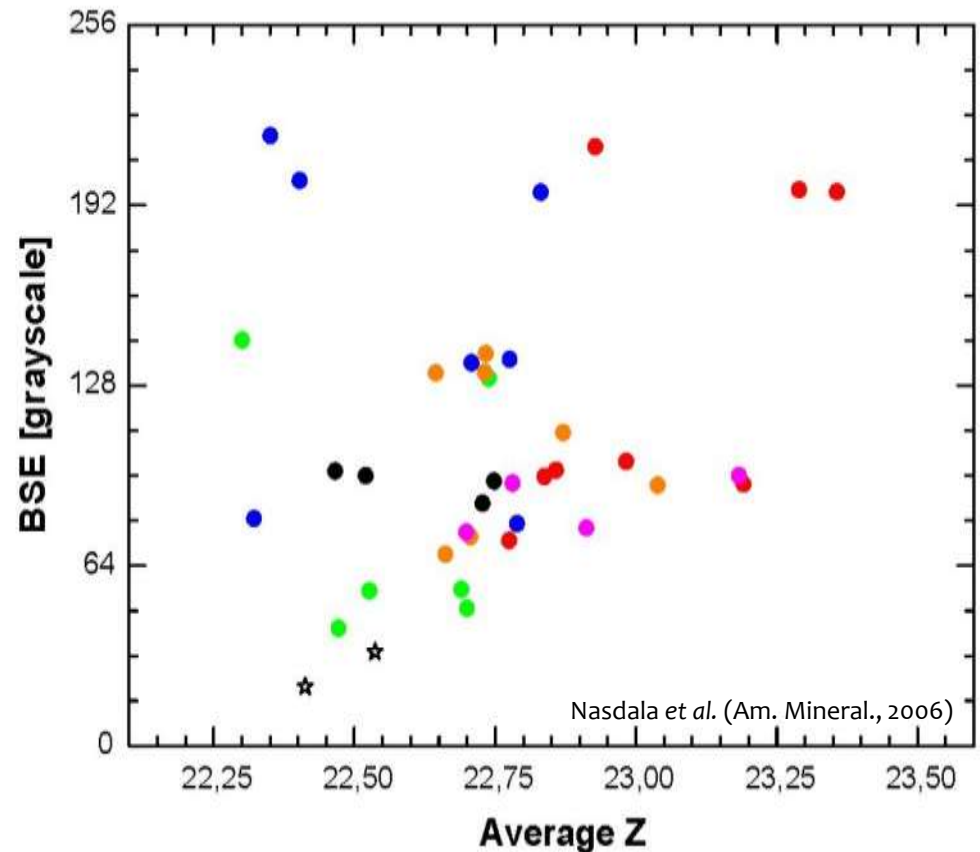
BSE contrast in zircon

BSE images of (unaltered) zircon single crystals:

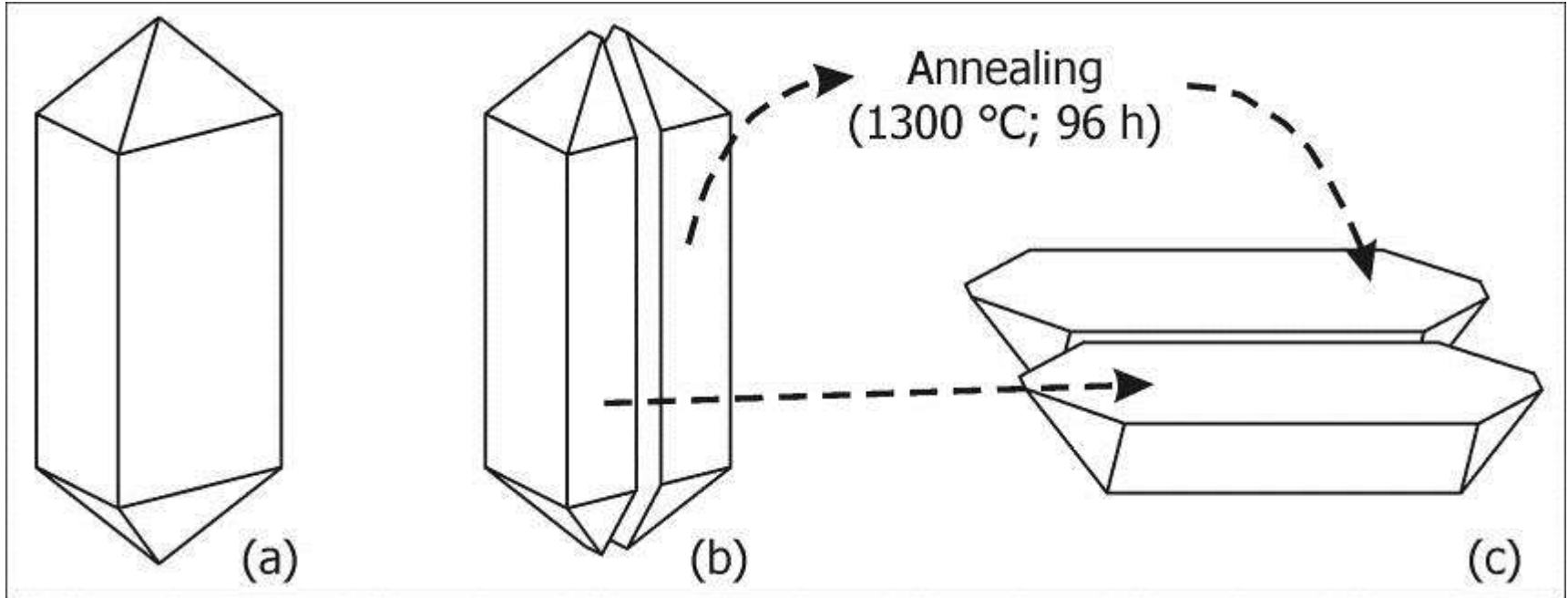
- no orientation contrast
- average Z contrast?



- Bluffpoint quartz diorite, Ontario (2732 Ma)
- Mulkahy Lake gabbro, Ontario (2733 Ma)
- Afella gneis, Algeria (1983 Ma)
- Leucogranite, Adirondacks (1045 Ma)
- Granite, Demitz, Saxony (530 Ma)
- Tuff, Hungary (19 Ma)
- ★ Synthetic zircon (0 Ma)

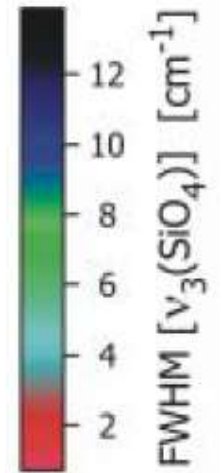
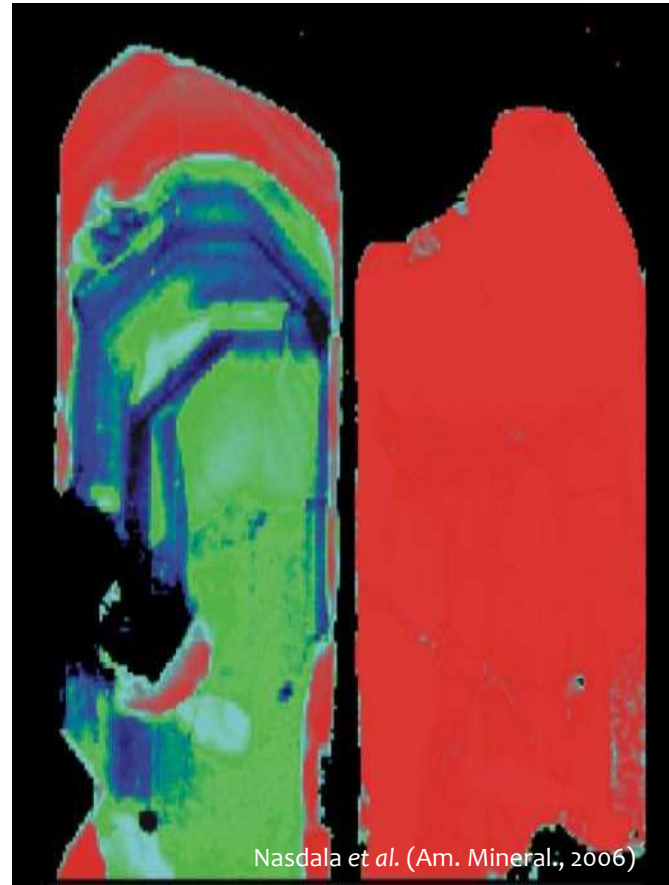
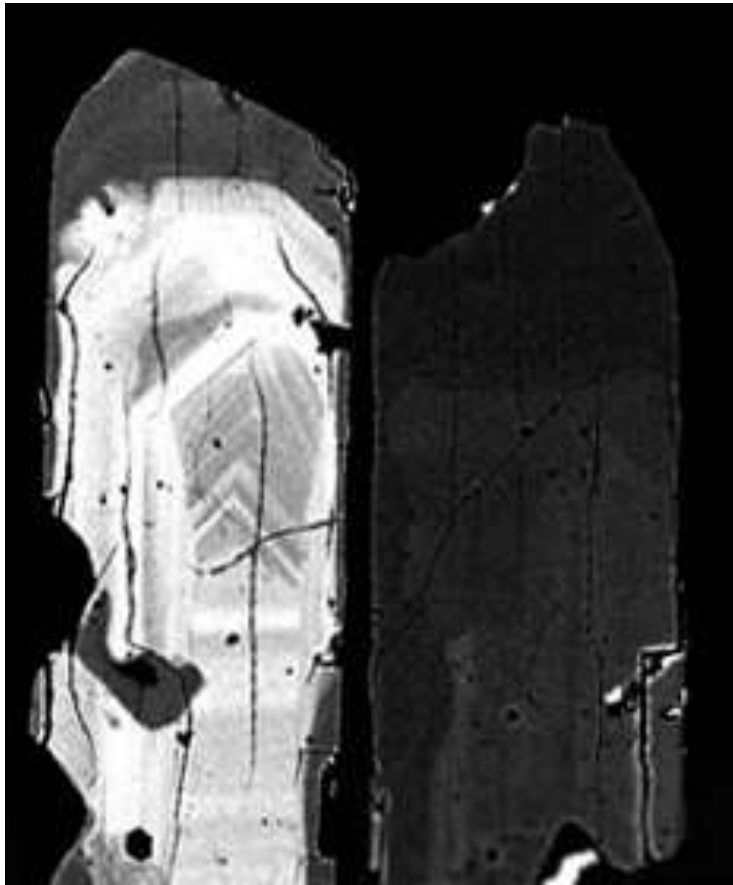


BSE contrast in zircon



- take a crystal
- cut it in two halves
- anneal one half
- mount and observe the two halves together

BSE contrast in zircon



50 μm

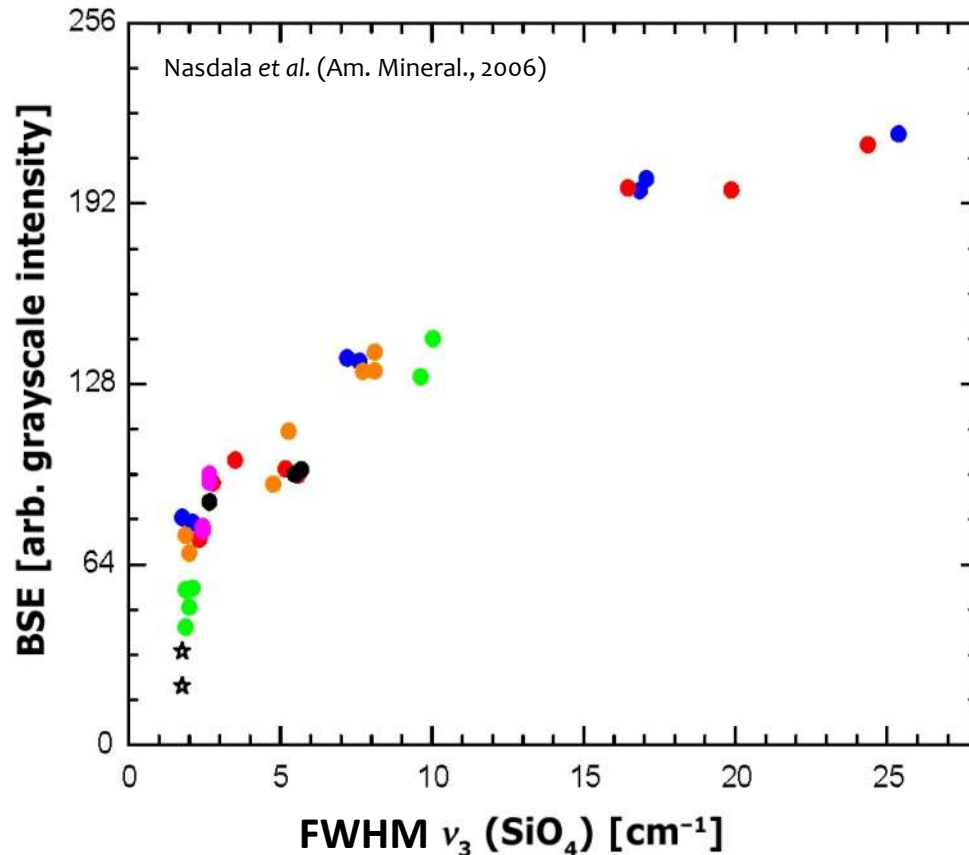
zircon crystal from Mulkahy Lake, Canada (sample D.W. Davis, Toronto)

BSE: grayscale image of backscattering coefficient

Raman map: Colour-coded representation of crystallinity

BSE contrast in zircon

- direct correlation between BSE intensity and the degree of radiation damage is observed



The contrast seen in BSE images of radiation-damaged, unaltered zircon crystals reflects the structural state, not chemical composition!

Electron-beam annealing

Váczai & Nasdala, *Phys. Chem. Mineral.*, in press

Electron-beam annealing

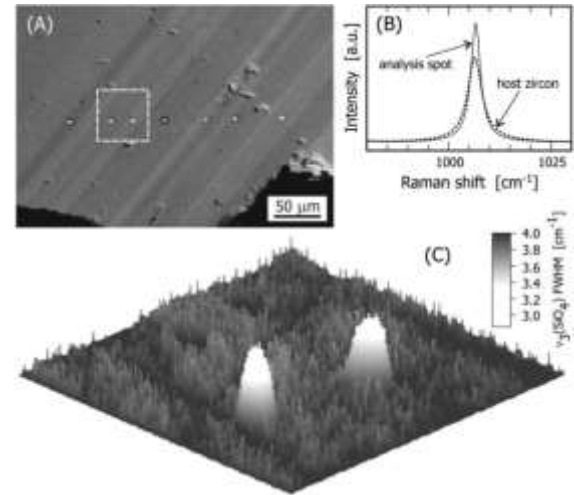
Electron microprobe analysis irradiates samples with moderate-energy electrons (typically 15–20 keV, up to 200 nA and 1000s of s)



+



=

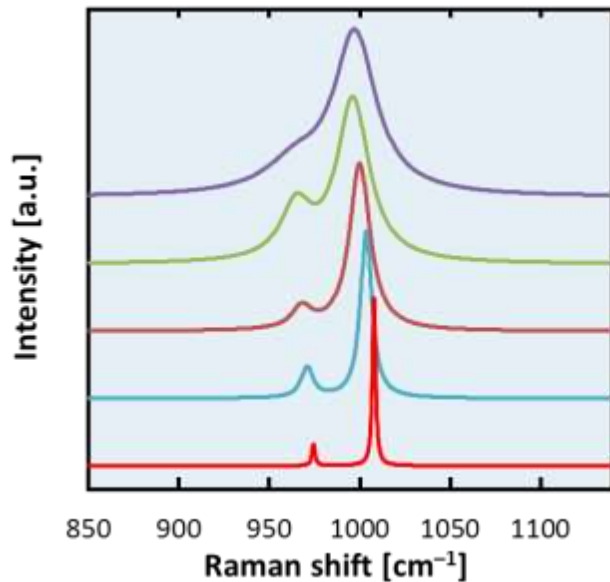


Zircon standard 91500
(from Nasdala et al., 2003)

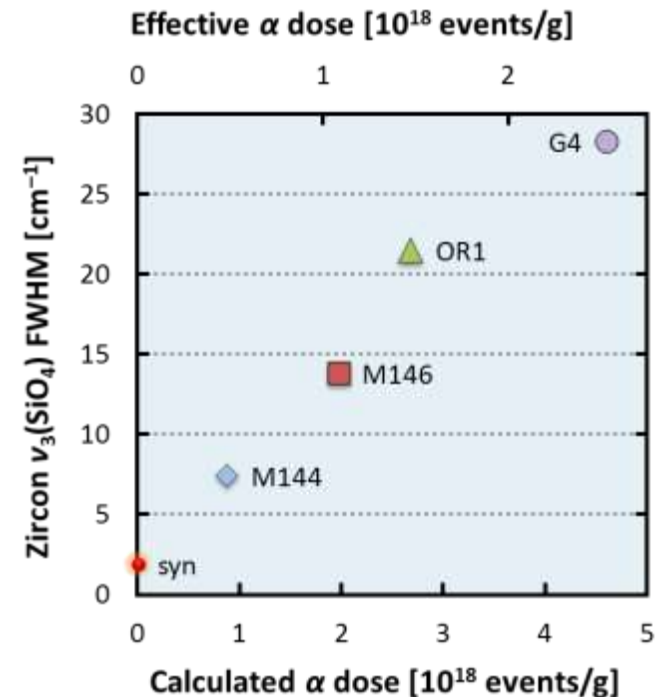
Raman spectroscopy: Irradiation with an electron beam induces an ordering of damage in zircon.

Electron-beam annealing

- Samples: gem-quality, homogeneous zircon fragments from Sri Lanka
- Note that Sri Lankan zircons do not show the damage corresponding to their calculated actinide content and age, a *ca.* $0.55\times$ correction is needed (Nasdala *et al.*, 2004)

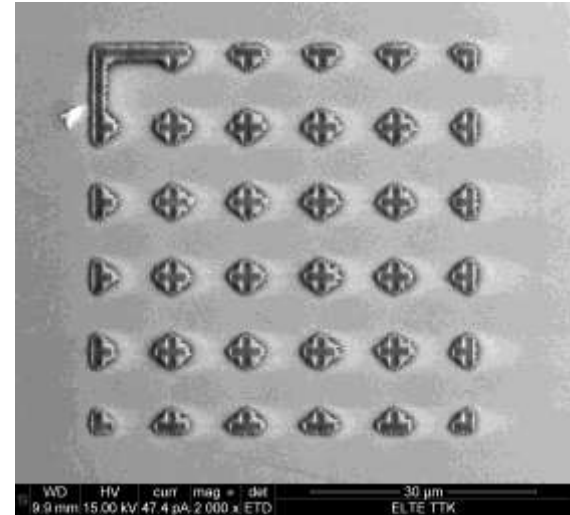


Sample	Effective α dose [10 ¹⁸ /g]
G4	2.46–2.70
OR1	1.44–1.61
M146	1.06–1.12
M144	0.47–0.50
syn	0

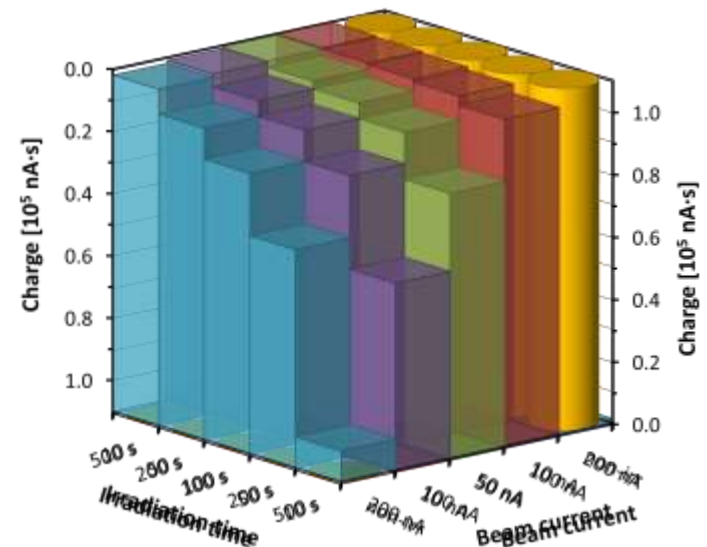


Electron-beam annealing

- Aim: a systematic evaluation of electron beam–zircon interaction
- EPMA (JEOL JXA-8600 Superprobe)
- fixed energy (20 keV)
beam current („flux“): 10 nA–200 nA
irradiation time: 10–500 s



	10 s	50 s	100 s	200 s	500 s
10 nA					
50 nA					
100 nA					
200 nA					
blank					



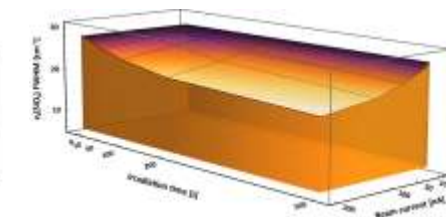
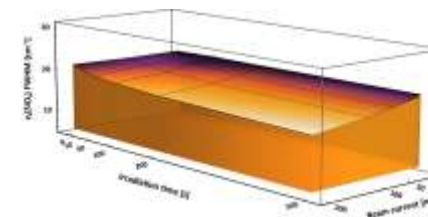
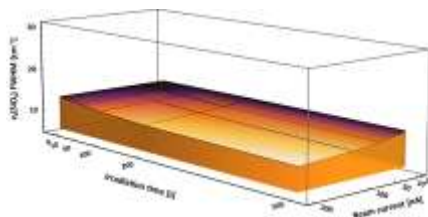
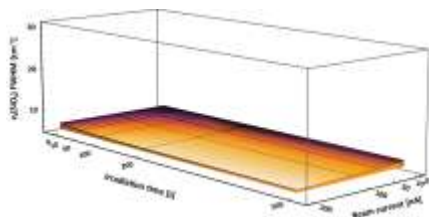
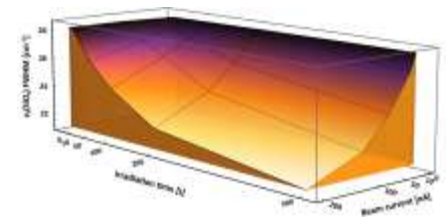
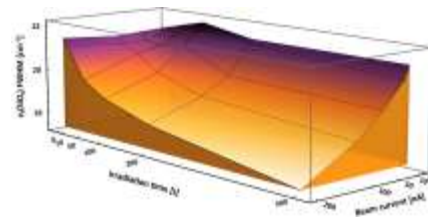
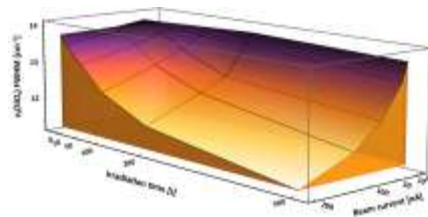
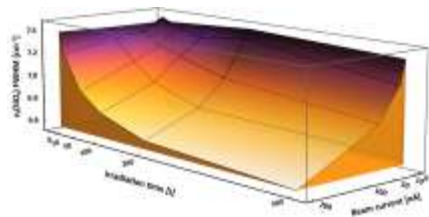
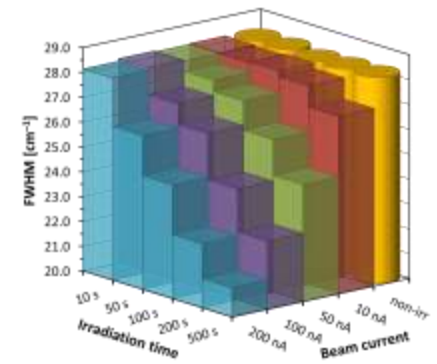
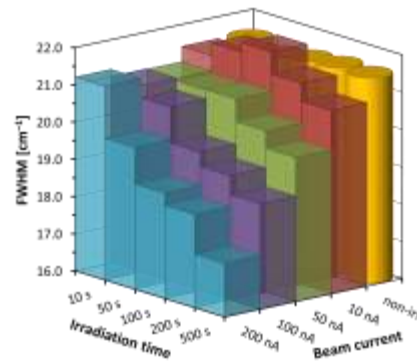
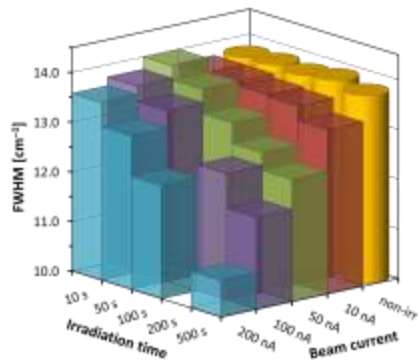
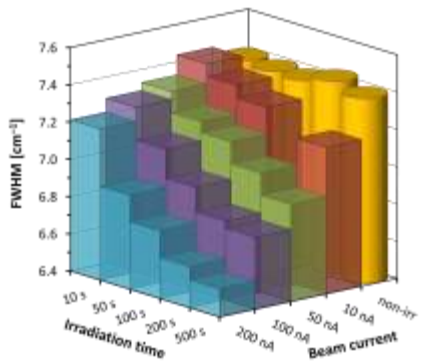
Electron-beam annealing

M144

M146

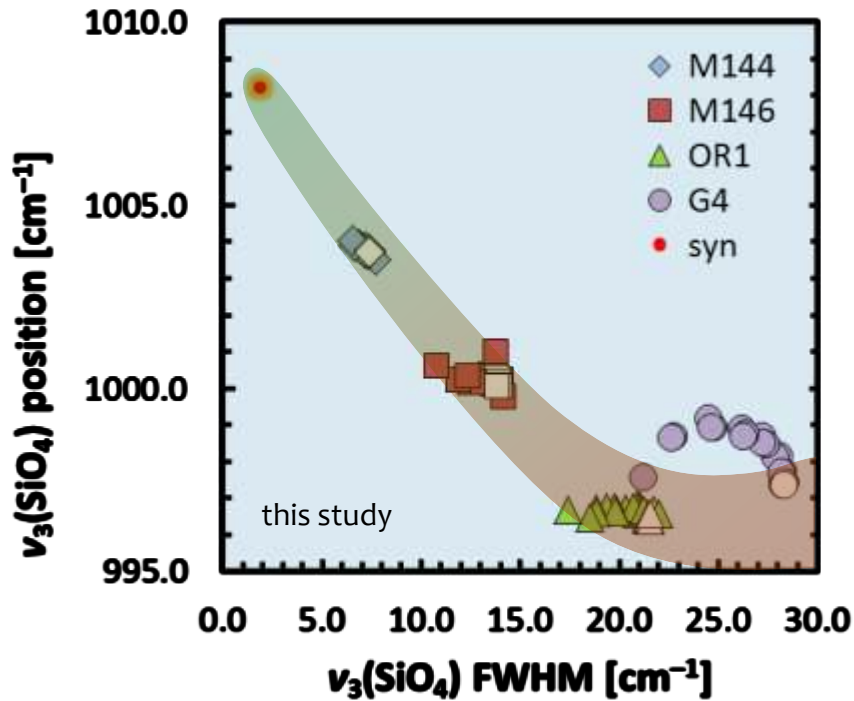
OR1

G4

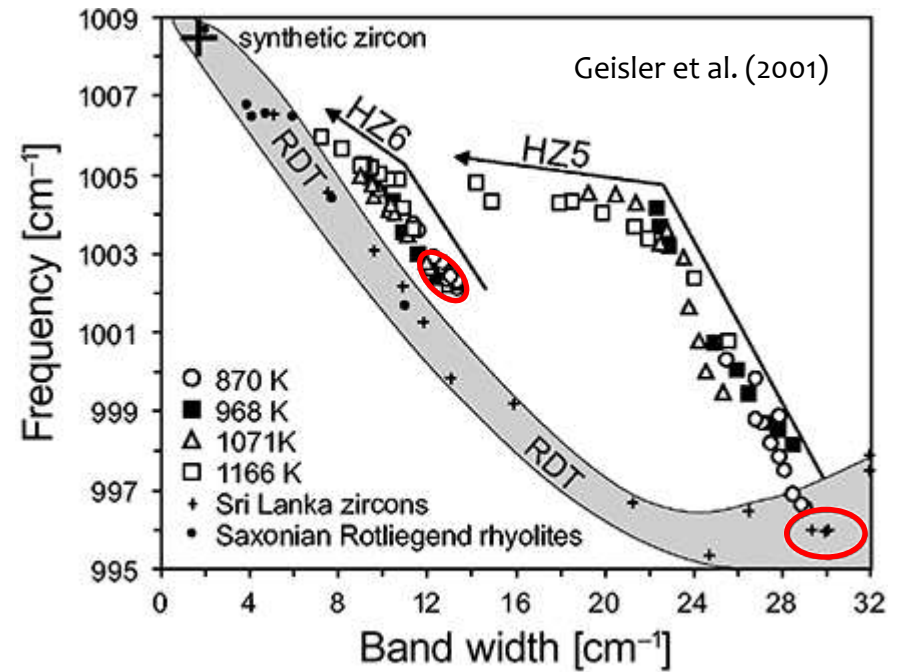


Electron-beam annealing

IF-deconvoluted and position-corrected data



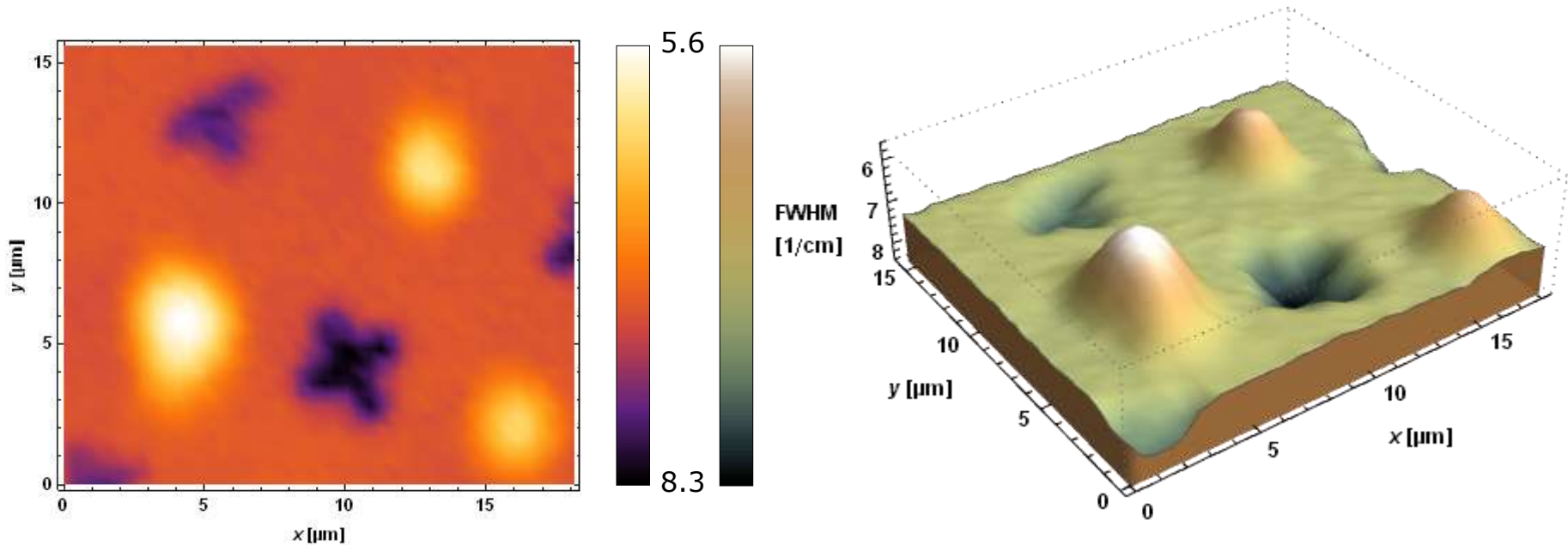
electron-beam annealing



thermal annealing

Electron-beam annealing

A detailed map can show annealing spots without positioning errors. (632.8 nm, ~13 mW, 46×40 steps/0.3 μm)



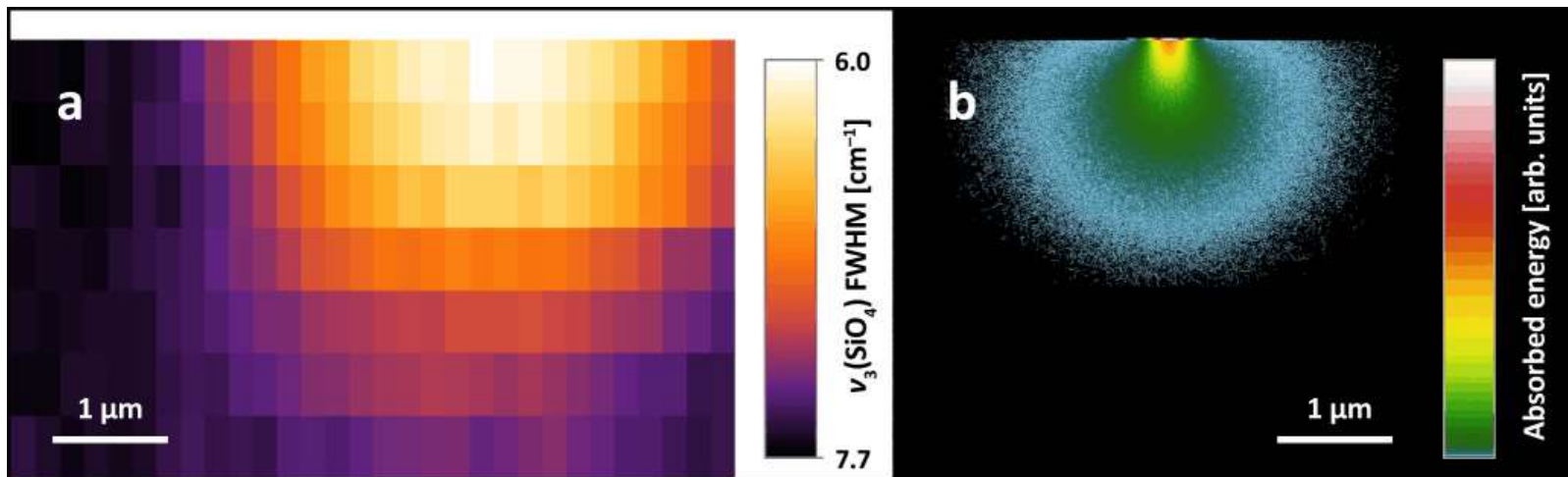
sample M144:

- 200 nA/500 s, 100 nA/500 s, 100 nA/200 s
- FIB-milled crosses

Electron-beam annealing

3D mapping: imaging of damage distribution in the depth of the electron-beam interaction volume

- surface focus is satisfactory
- small electron energies still appear to anneal damage (633 nm, ~13 mW, 20×40 steps/0.2 μm x-y, 8 steps/0.5 μm z)



x-z section of
3D FWHM map

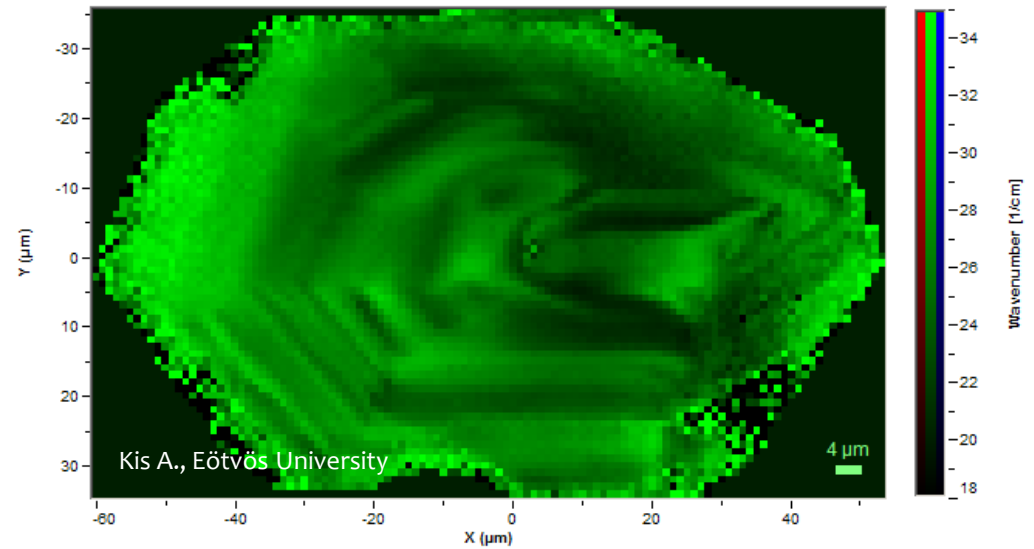
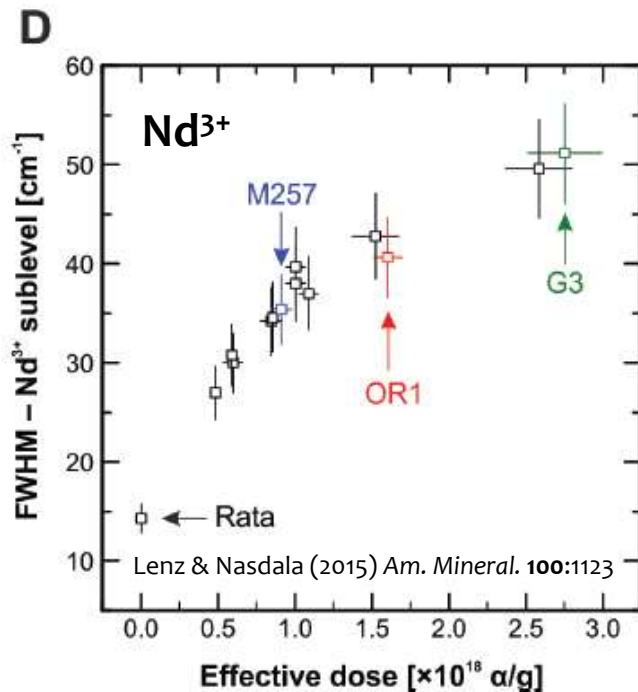
CASINO MC simulation
of energy transfer

PL mapping



PL mapping

REE PL emissions probe the crystal field around the $\text{V}^{\text{III}}\text{Zr}$ site.



PL map (532 nm, 4 mW, 2×8 s, 114×70 steps/ $1 \mu\text{m}$)

Free advice: NEVER forget the “f”!

